

Resonance enhancement of neutrinoless double electron capture

M.I. Krivoruchenko^{a,b}, Fedor Šimkovic^{c,d}, Dieter Frekers^e, Amand Faessler^f

^a*Institute for Theoretical and Experimental Physics, B. Chermushkinskaya 25
117218 Moscow, Russia*

^b*Department of Nano-, Bio-, Information and Cognitive Technologies
Moscow Institute of Physics and Technology, 9 Institutskii per.
141700 Dolgoprudny, Moscow Region, Russia*

^c*Bogoliubov Laboratory of Theoretical Physics, JINR
141980 Dubna, Moscow Region, Russia*

^d*Department of Nuclear Physics and Biophysics, Comenius University
Mlynská dolina F1, SK-842 48 Bratislava, Slovakia*

^e*Institut für Kernphysik, Universität Münster, Wilhelm-Klemm-Str. 9
48149 Münster, Germany*

^f*Institut für Theoretische Physik, Tübingen Universität, Auf der Morgenstelle 14
D-72076 Tübingen, Germany*

Abstract

The process of neutrinoless double electron ($0\nu\text{ECEC}$) capture is revisited for those cases where the two participating atoms are nearly degenerate in mass. The theoretical framework is the formalism of an oscillation of two atoms with different total lepton number (and parity), one of which can be in an excited state so that mass degeneracy is realized. In such a case and assuming light Majorana neutrinos, the two atoms will be in a mixed configuration with respect to the weak interaction. A resonant enhancement of transitions between such pairs of atoms will occur, which could be detected by the subsequent electromagnetic de-excitation of the excited state of the daughter atom and nucleus. Available data of atomic masses, as well as nuclear and atomic excitations are used to select the most likely candidates for the resonant transitions. Assuming an effective mass for the Majorana neutrino of 1 eV, some half-lives are predicted to be as low as 10^{22} years in the unitary limit. It is argued that, in order to obtain more accurate predictions for the $0\nu\text{ECEC}$ half-lives, precision mass measurements of the atoms involved are necessary, which can readily be accomplished by today's high precision Penning traps. Further advancements also require a better understanding of high-lying excited states of the final nuclei (i.e. excitation energy, angular momentum and parity) and the calculation of the nuclear matrix elements.

Keywords: neutrino mass, neutrinoless double beta decay, double electron capture, nuclear matrix elements

1. Introduction

The question as to whether massive neutrinos obey a Dirac or a Majorana symmetry, presently constitutes one of the most important unresolved problems of particle physics and astrophysics. If neutrinos are Dirac particles, i.e. if neutrino and antineutrino are fundamentally different, then total lepton number $L = L_e + L_\mu + L_\tau$ must be conserved. Contrary, if neutrinos are Majorana particles, i.e. if neutrino and antineutrino are identical particles, then lepton number conservation is not required anymore. Indeed, lepton number (LN) conservation is one of the most obscure appearances in the Standard Model of elementary particles, since there is no known fundamental principle or symmetry, which would require this.

Already in 1939 Furry [1] noticed that the exchange of neutrinos (later termed Majorana neutrinos) between two neutrons could lead to the production of two protons and two electrons in the reaction

$$(A, Z) \rightarrow (A, Z + 2) + e^- + e^-. \quad (1.1)$$

Today, such a reaction is termed the neutrinoless double-beta ($0\nu\beta\beta$) decay, and an observation of this reaction is still the only unambiguous way to identify the Majorana character of the neutrino [2]. Over the years, considerable efforts from experimentalists and theorists alike have been devoted to this process (for reviews see Ref. [3]). Although of fundamental importance, this process is unfortunately characterized by an excessively low rate, which poses a significant challenge to any experiment.

Assuming that the light neutrino mixing mechanism provides the dominant contribution to the $0\nu\beta\beta$ -decay, the decay rate for a given isotope (A, Z) is simply given by the product of the effective Majorana neutrino mass squared $|m_{\beta\beta}|^2$, the known 3-body phase-space factor, and the much less well-known nuclear matrix element squared, which is particular to every nuclear transition under study. The phase-space factor contains a dependence on the nuclear charge Z ($\sim Z^2$), the Q-value of the reaction ($\sim Q^5$) and the Fermi-coupling constant ($\sim G_F^4$). The main objective of every experimental $0\nu\beta\beta$ -decay search is the determination of the absolute value of the effective Majorana neutrino mass $|m_{\beta\beta}|$. However, a mere observation of the decay would already constitute a significant advancement in neutrino physics.

In the 3-neutrino mixing scenario, the effective Majorana neutrino mass $m_{\beta\beta}$ takes the form

$$m_{\beta\beta} = \sum_{i=1}^3 U_{ei}^2 m_i. \quad (1.2)$$

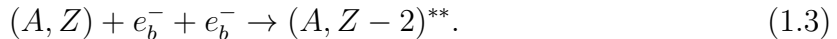
Here, U_{ei} ($i = 1, 2, 3$) are the elements of the Pontecorvo-Maki-Nakagawa-Sakata (PMNS) neutrino mixing matrix, which mixes the mass eigenstates m_i in weak interaction. It contains the usual 3-neutrino mixing angles plus a CP-violating phase, which appears in oscillations, and two additional Majorana phases, ϕ_1, ϕ_2 .

The recent claim for an observation of the $0\nu\beta^-\beta^-$ -decay of ^{76}Ge with $T_{1/2}^{0\nu} = 2.23_{-0.31}^{+0.44} \times 10^{25}$ years [4] implies $|m_{\beta\beta}| \simeq 0.18 - 0.30$ eV by assuming the renormalized QRPA (RQRPA) nuclear matrix element and its uncertainty given in Ref. [5].

The goal of the upcoming GERDA experiment [6] is to put this claim to a test by improving the sensitivity limit of the detection by more than an order of magnitude. The next generation experiments, which will be using several other candidate nuclei, will eventually be able to achieve this goal as well [7].

The value of the effective Majorana mass, as it appears in Eq. (1.2), contains several dependencies on phases and masses. Because of experimental uncertainties, different mass scenarios, like the normal ($m_3 \gg m_2 \gg m_1$) or inverted ($m_2 > m_1 \gg m_3$) hierarchy scenario, or degenerate ($m_3 \approx m_2 \approx m_1$) or non-degenerate cases, can presently still be entertained, which allow a wide range of possible mass values for $|m_{\beta\beta}|$, even zero in the most extreme and unfortunate situation of the normal hierarchy scenario [8]. Though even in that case the $0\nu\beta\beta$ will still be allowed due to a contribution from the mass term in the neutrino propagator [9], which one usually neglects, its decay rate would be utterly unobservable.

Recently, there has been an increased theoretical and experimental interest to another LN violating process, which is the neutrinoless double electron capture ($0\nu\text{ECEC}$) [10, 11, 12, 13]. In this reaction two bound electrons from the atomic shell are captured by two protons, thereby lowering the charge of the final nucleus by two units:



Here, the two asterisks denote the possibility of leaving the system in an excited nuclear and/or atomic state, the latter being characterized by two vacancies in the electron shell of the otherwise neutral atom. The energy excess given by the Q-value of the reaction must still be carried away by an extra photon, in order to conserve energy. This is unlike the 2-neutrino case, where the neutrinos can provide the energy balance. Thus, the reaction in Eq. (1.3) could in principle be detected by monitoring the X-rays or Auger electrons emitted from excited electron shell of the atom, the electromagnetic decay of the excited nucleus (in case of a non-ground-state transition) and the extra photon, whose energy would be

$$E_{h\nu} = Q - E_{\text{atom}}^x - E_{\text{nucl}}^x. \quad (1.4)$$

We note that $0\nu\text{ECEC}$ was considered by Winter [14] already in 1955.

The signature of the $0\nu\text{ECEC}$ process is, therefore, different from the signature of the $0\nu\beta\beta$ decay and would also require rather different coincident detection techniques. On the other hand, the coupling to an extra photon and/or X-ray clearly makes the half-life excessively long to the extent that this process has not been considered a valid experimental option altogether.

The situation changes, however, if the energy difference in Eq. (1.4) approaches zero and no extra photon is required. This has been discussed by Bernabéu, De Rujula, and Jarlskog [15], who pointed to the possibility of a resonant enhancement of the $0\nu\text{ECEC}$ decay in case of a mass degeneracy between the initial and final nucleus. Their best candidate case was ^{112}Sn , where the $0\nu\text{ECEC}$ double K-shell capture process would lead to an excited 0^+ state at 1871 keV in the final nucleus ^{112}Cd . This possibility was recently excluded by a new mass difference measurement

performed at Jyväskylä ($\Delta M = 1919.82(16)$ keV) [16], where it was shown that the energy to be paid by the double K-shell vacancy would not leave enough energy available for the excitation of the 1871 keV state in ^{112}Cd .

The $0\nu\text{ECEC}$ decays became a subject to a detailed theoretical treatment by Sujkowski and Wycech [10], who used a perturbative approach. Their conclusion was that an exact energy degeneracy could make the $0\nu\text{ECEC}$ reaction competitive to the $0\nu\beta^-\beta^-$ -decay. However, a case with an exact energy degeneracy could not be identified.

Recently, another case for a near mass-degeneracy was found and discussed in Ref. [11]. Here, it was argued that the 1204 keV state in ^{74}Ge would be nearly degenerate to the ground state of the atomic nucleus ^{74}Se in case of a double L-capture process and given the experimental errors on the masses. A new mass difference measurement performed by Kolhinen *et al.* [17] essentially confirmed the previous central mass difference value of $\Delta M = 1209.169(49)$ keV, however, with much higher precision. These authors therefore excluded a complete mass degeneracy with the 1204 keV state in ^{74}Ge , even in the case of a double L-capture, where the atomic energy for a double L-vacancy would amount to an extra 2.9 keV on top of the 1204 keV [11]. Prior to this, two experiments had already been performed by Barabash *et al.* [12, 13], which gave lower bounds for the half-lives of ^{74}Se and ^{112}Sn :

$$\begin{aligned} T_{1/2}^{0\nu\text{ECEC}}(^{74}\text{Se}) &\geq 5.5 \times 10^{18} \text{ y}, \\ T_{1/2}^{0\nu\text{ECEC}}(^{112}\text{Sn}) &\geq 9.2 \times 10^{19} \text{ y}. \end{aligned}$$

In this paper we present a new theoretical framework for the calculation of resonant $0\nu\text{ECEC}$ transitions, namely the oscillation of atoms. An improved theoretical description of the process includes the determination of relevant matrix elements for the most favored cases of capture of the $s_{1/2}$ and $p_{1/2}$ electrons. The $0\nu\text{ECEC}$ transitions without and with the spatial parity violation are considered. Further, we provide an updated list of the most likely resonant transitions taking new nuclear spectroscopic data into account and using recent accurate measurements of Q values for several nuclei [17, 16, 18, 19, 20, 21]. The selection of transitions is also based on accurate treatment of spin-tensor structures that arise in a product of the nuclear matrix elements and the electron wave functions of atomic shells. The reverse reaction

$$(A, Z) \rightarrow (A, Z + 2)^{**} + e_b^- + e_b^- \quad (1.5)$$

of a neutrinoless production of two bound electrons ($0\nu\text{EPEP}$) will also be discussed.

The outline of the paper is as follows: First we discuss the mixing of atoms with different lepton charges. This effect leads to the oscillations of atoms. In Sect. 2, we discuss the relevant formalism of the oscillations. We will show that the oscillation of stable atoms produces a too small effect to be measured experimentally. However, oscillation between a stable and an excited atom can lead to a resonant enhancement of lepton number violating decays.

Sect. 3 presents the estimated half-lives of the decays. In the calculations we use the data on the Auger and radiative widths of excited electron shells and the

information on the Coulomb interaction energy of two electron holes. We consider nuclei with arbitrary spin-parity and take into account the fact that the spin-parity uniquely determines a combination of upper and lower components of the relativistic electron wave functions entering the matrix elements associated with the capture. In Appendix A the procedure of averaging the electron wave functions over the nucleus is discussed. The transition matrix elements are derived for the $J_f^\pi = 0_f^\pm$ and 1_f^\pm states of the daughter nuclei in Appendix B. The problem of calculating matrix elements is very complicated, and the result depends sensitively on the particular transition. We identify the most promising nuclei in the search for 0ν ECEC decays. Such nuclei will continue to be analyzed in future. In this paper, the half-lives are normalized to the nuclear matrix element $\mathcal{M}^{0\nu}(0_i^+ \rightarrow J_f^\pi) = 6$, which is close to the maximum evaluated value of the matrix elements for medium-heavy nuclei. In Sect. 3, we also give a complete list of the most likely resonance transitions, in which the unitary limit of resonant enhancement gives half-lives of less than 10^{27} years for $|m_{\beta\beta}| = 1$ eV. We argue that accurate measurements of the mass differences between initial and final states of the nuclei are necessary, if future experiments of 0ν ECEC decays with half-lives below 10^{27} years were to become a possibility. Experimental signatures of 0ν ECEC decays are discussed in Sect. 4.

2. Lepton number violating transitions between ground state and excited atoms

If lepton number is not conserved, then the weak interaction mixing between a pair of neutral atoms (A, Z) and $(A, Z \pm 2)$ is a natural occurrence, which leads to an oscillation between these two many-body quantum systems. In the present description we focus on a system, in which one of the atoms (usually the daughter atom) is left in an excited atomic or nuclear state. In fact, for EC processes the daughter atomic system is always excited, as the capture process always leaves a vacancy in the electron shell. If the ECEC Q-value is of the order of the excitation of the atomic shell with two electron vacancies, one may expect a resonant-like transition. A few examples do exist in the nuclear chart, which have this property. On the other hand, if the ECEC Q-value is significantly larger than the atomic excitation, one may find a situation, where an excited nuclear state matches the available energy (i.e. $Q - E_{\text{atom}}^x = E_{\text{nucl}}^x$), allowing again a resonant-like transition to an excited nuclear state. The latter type of oscillations may even have a practical experimental signature: one or even several X-ray photons or Auger electrons from the de-excitation of the atomic shell being coincident with a γ -ray (or a cascade of γ -rays) from the de-excitation of the nucleus. In fact, the detection of a coincident γ -ray cascade, if existent, may already be sufficient to uniquely identify the transition. It may be worth re-iterating that any such transition requires the neutrino to be of Majorana type, as there is no phase space available for the emission two extra neutrinos.

The present description of a resonant enhancement of the ECEC transition will be done in the context of oscillations. We wish to point out, that our results are consistent with the results of Bernabéu et al. [15] and Sujkowski and Wycech [10] for

the physically interesting case, where the frequency of oscillations is much smaller than the width of the excited atom. In the opposite limit, when the frequency of oscillations is high, the standard formulas of the time evolution of a two-level system are retained.

2.1. Oscillations in arbitrary systems

Specific features of the oscillations in the system of two atoms were discussed earlier in Ref. [22]. Two coupled oscillators, one of which experiences friction, constitute the mechanical analogue of the system, which we are considering.

Lepton number violating interactions induce transitions $(A, Z) \rightarrow (A, Z \pm 2)^{**}$. These transitions can be described phenomenologically by 2×2 non-Hermitian Hamiltonian matrix

$$H_{\text{eff}} = \begin{pmatrix} M_i & V \\ V^* & M_f - \frac{i}{2}\Gamma \end{pmatrix}. \quad (2.1)$$

Here M_i and M_f are the masses of the initial and final atom. Γ is the decay width of the excited daughter atom. The off-diagonal matrix elements of H_{eff} are complex conjugate. The transition potential V can always be made real by changing the phase of one of the states, i.e. $V = V^*$. The diagonal matrix elements of the Hamiltonian are determined by strong and electromagnetic interactions, which conserve lepton number. The off-diagonal elements provide the mixing of the neutral atoms, and thereby, violate lepton number by two units as a result of the weak interaction with massive Majorana neutrinos. Using the Pauli matrices, the Hamiltonian can be written as:

$$H_{\text{eff}} = M_+ + V\sigma_1 + M_-\sigma_3, \quad (2.2)$$

where

$$M_{\pm} = \frac{M_i \pm M_f}{2} \mp \frac{i}{4}\Gamma. \quad (2.3)$$

The evolution operator $e^{-iH_{\text{eff}}t}$ can be expanded over the Pauli matrices to give

$$e^{-iH_{\text{eff}}t} = e^{-iM_+t} \left(\cos(\Omega t) - i \frac{V\sigma_1 + M_-\sigma_3}{\Omega} \sin(\Omega t) \right), \quad (2.4)$$

where $\Omega = \sqrt{V^2 + M_-^2}$.

One can see that all components of the evolution operator behave like $e^{-i\lambda_{\pm}t}$, with $\lambda_{\pm} = M_+ \pm \Omega$. Since the eigenfrequencies λ_{\pm} are complex, the norm of the states is not preserved in time.

A somewhat similar form of the 2×2 Hamiltonian matrix is responsible for the oscillation of neutral kaons [23]. The main difference between the oscillation of neutral atoms and that of kaons is the mixing, which is maximum for kaons and exceedingly small for atoms.

The Hamiltonian in Eq. (2.1) also describes the effect of neutron-antineutron oscillation in nuclear matter [24, 25]. In this case, M_i and M_f would be the neutron and antineutron masses, V the baryon number violating potential, and Γ the antineutron width related to annihilation channels (in vacuum $M_i = M_f$ and $\Gamma = 0$).

The formalism is also similar to the one used for describing oscillations and decays of unstable neutrinos [26].

2.2. Oscillations of two stable atoms

If the two atoms are stable, then $\Gamma = 0$ and $\Omega = (M_i - M_f)/2$. The transition probability is determined by the off-diagonal matrix element of the evolution matrix (2.4):

$$|\langle f|e^{-iH_{\text{eff}}t}|i\rangle|^2 = \frac{V^2}{\Omega^2} \sin^2(\Omega t). \quad (2.5)$$

This is just the case of oscillations of a two-level system described for instance in Ref. [27]. If $\Omega t \ll 1$, the transition probability $\sim V^2 t^2$ is determined by the potential V only. However, the exposure time of atoms in double β -decay experiments (months and years) is greater than $1/\Omega$ by many orders of magnitude. By taking the average over one period, we one arrives at

$$|\langle f|e^{-iH_{\text{eff}}t}|i\rangle|^2 \approx \frac{2V^2}{(M_i - M_f)^2}. \quad (2.6)$$

In the transitions $(A, Z) \leftrightarrow (A, Z \pm 2)$, the composition of valence electron shells changes and, thus, the chemical properties of the substance. This circumstance can in principal be used for registering the oscillations of atoms. However, the potential V is at least 30 orders of magnitude smaller than the atomic mass difference. For a hypothetical mass difference of $M_i - M_f \approx 10$ keV one finds $|\langle f|e^{-iH_{\text{eff}}t}|i\rangle|^2 < 10^{-60}$. Since degenerate ground-state masses do not exist, this scenario is purely academic, and we turn to systems of a stable mother and an excited daughter atom.

2.3. Oscillations and resonant transitions between ground state and excited atoms

According to the arguments in Ref. [22], we assume a potential strength of $V \sim 10^{-24}$ eV, a typical decay width of $\Gamma \sim 1$ eV for a medium-heavy atom, and a typical mass difference of $(M_i - M_f) \sim 1$ MeV. In the lowest order in V , we obtain

$$\lambda_+ = M_i + \Delta M - \frac{i}{2}\Gamma_1, \quad (2.7)$$

$$\lambda_- = M_f - \frac{i}{2}\Gamma - \Delta M + \frac{i}{2}\Gamma_1, \quad (2.8)$$

where

$$\Delta M = \frac{V^2(M_i - M_f)}{(M_i - M_f)^2 + \frac{1}{4}\Gamma^2}, \quad (2.9)$$

$$\Gamma_1 = \frac{V^2\Gamma}{(M_i - M_f)^2 + \frac{1}{4}\Gamma^2}. \quad (2.10)$$

Since the width Γ_1 is small, the imaginary parts of λ_{\pm} in Eqs. (2.7) and (2.8) are negative, therefore, the states decay. Equation (2.10) gives the decay rate of the initial atom in agreement with the Breit-Wigner formula.

The excited atom manifests itself as a resonance in the decay amplitude. The most favorable conditions for the detection of the violation of lepton number conservation occur in the transitions $(A, Z) \rightarrow (A, Z - 2)^*$, where the masses of the initial

and final states are equal (degenerate) and the decay width of the daughter atomic nucleus is small.

The amplitude of finding the initial atom t seconds after its preparation in the same initial state is determined by the diagonal matrix element of the evolution operator:

$$\langle i | e^{-iH_{\text{eff}}t} | i \rangle = e^{-i\lambda_- t} \frac{V^2}{4M_-^2} + e^{-i\lambda_+ t} \left(1 - \frac{V^2}{4M_-^2}\right). \quad (2.11)$$

The second term oscillates with the frequency $\approx M_i$ and decays with the rate Γ_1 . At a low frequency, the system is unable to return to the initial state and decays. In this case one can talk about a lepton number violating decay of the initial atom with a width Γ_1 (Eq. 2.10).

The decay width Γ_1 reaches the unitary limit

$$\Gamma_1^{\text{max}} = \frac{4V^2}{\Gamma} \quad (2.12)$$

in the case of a complete degeneracy between initial and final state. From an experimental standpoint, where one would search for such lepton number violating decays, this would be the case of highest interest.

3. Analysis of $0\nu\text{ECEC}$ half-lives throughout periodic table

The selection of atomic systems with the potentially shortest $0\nu\text{ECEC}$ half-lives is based on equation (2.10). The equation shows that the decay rate is determined by three quantities: the mass difference between the initial and final states, the decay width of the final state, and the transition potential.

The mass difference depends on the Q-value of the ECEC decay and the energy of the two electron vacancies in the final atom. In atomic physics, the electron binding energies can usually be calculated with an accuracy of several eV. We borrowed the binding energies from Ref. [28]. Noticeable corrections will, however, arise from the Coulomb interaction of the two holes. These calculations are carried out on the basis of the Dirac equation taking into account the screening effects of the nuclear charge.

The decay width of the final atom is determined by the dipole emission rate leading to the de-excitation of the electron shell. In the nonrelativistic approximation, the capture rates of two electrons from the higher shells, like L, M, or N shells, scale with the principal quantum numbers n_1, n_2 as $(\alpha Z/n_1)^3(\alpha Z/n_2)^3$, but we will see that in the unitarity limit of a resonant decay this strong reduction of the probability could possibly be compensated by smallness of the de-excitation rates. The total decay width of the system is given by the sum of the widths of the atomic and the nuclear state. In most cases the decay width of the excited nucleus is smaller than the one of the atomic state by at least an order of magnitude and can, therefore, be neglected. The process of Auger electron emission as the alternative de-excitation process of the atom is also taken into account following the results of Ref. [29]. The Auger electron emission is faster than the electromagnetic decays for low atomic Z .

The transition potential contains the uncertainties of the transition matrix elements connected with the complicated structure of the nuclear excitation. In order to obtain numerical estimates, we factorize the $0\nu\text{ECEC}$ matrix element on a product of the atomic physics factor and the nuclear matrix element. This simplification is justified due to weak radial dependence of the $s_{1/2}$ and $p_{1/2}$ electron wave functions inside nuclei. Further, we normalize all the $0\nu\text{ECEC}$ nuclear matrix elements to the value of nuclear matrix element obtained for the ground state to ground state transition $^{152}_{64}\text{Gd} \rightarrow ^{152}_{62}\text{Sm}$ in Ref. [30]. The contributions from the electron shell are determined by different combinations of the relativistic wave functions of electrons for the capture from different shells. We systematically examine transitions between all the states $|J_f - J_i| = 0, 1, 2, \dots$ with the parities $\pi_f \pi_i = \pm 1$ for the capture of two electrons with orbital angular momenta $0 \leq l_1 + l_2 \leq 2$ and the principal quantum numbers $1 \leq n_1, n_2 \leq 4$.

3.1. Coulomb interaction energy of electron holes

The binding energy of electrons in the inner atomic shells varies from 10 eV in light nuclei up to 100 keV in heavy nuclei. In the outer shells, the binding energy is a few eV, both in light and heavy nuclei. Since electrons are usually captured from the most inner shells, the electron binding energy gives sizeable contribution to the energy balance in the double electron capture. We use data of electron binding energies reported by Larkins [28]. Those are accurate to better than an eV for light nuclei and to a few tens of eV in heavy nuclei. The relevant binding energies in the context of ECEC are, of course, always those for the final daughter atom with $Z - 2$.

In heavy elements, the electron hole interaction energies may reach values of a few keV (for a double K-shell vacancy), which is quite large for our problem in question. It is therefore essential to calculate the interaction energies of two electron holes and include them into the total energy equation.

We used an approach that takes screening of the Coulomb potential by electrons occupying other orbitals into account. The shielding effect can be estimated from the known energy ε of the bound electrons. In the non-relativistic theory, the effective charge Z_* can be found from equation

$$\varepsilon = m - \frac{\alpha^2 Z_*^2}{2n^2} m, \quad (3.1)$$

where m is the electron mass, n is the principal quantum number. In the non-relativistic theory, the electron velocity $v \sim \alpha Z/n$ increases with the nuclear charge, which requires a relativistic treatment for heavy nuclei.

The binding energies in the Coulomb field are known from the Dirac relativistic wave equation [31]. Given ε , the effective charge may be found from

$$\alpha^2 Z_*^2 = \frac{\lambda^2}{m^2} \left(\kappa^2 + n_r^2 - 2n_r \frac{n_r \lambda^2 - \varepsilon \sqrt{-n_r^2 \lambda^2 + \kappa^2 m^2}}{m^2} \right), \quad (3.2)$$

where $\lambda = \sqrt{m^2 - \varepsilon^2}$, $\kappa = -(2j + 1)(j - l)$, $j = l \pm 1/2$, and $n_r = n - (j + 1/2) \geq 0$. Near the limit of $\varepsilon \rightarrow m$, the non-relativistic formula is recovered.

The effective charge $Z_* < Z$ takes into account the screening of the Coulomb potential, as well as the finite nuclear size. Given that the electron-shell wave functions are known, one can calculate the interaction energy of electron holes.

We consider transitions between nuclei with good quantum numbers J^π , so the two-electron wave function should have good total angular momentum J , projection M , and parity. This can be arranged by weighting the two-electron wave function with the Clebsch-Gordan coefficients

$$\psi_{\beta\delta}^{JM}(\mathbf{x}_1, \mathbf{x}_2) = \sum_{m_\beta m_\delta} C_{j_\beta m_\beta j_\delta m_\delta}^{JM} \Psi_{\beta m_\beta}(\mathbf{x}_1) \Psi_{\delta m_\delta}(\mathbf{x}_2). \quad (3.3)$$

Here, $\Psi_{\alpha m_\alpha}(\mathbf{x})$ ($\alpha = (njl)$) is the relativistic wave function of the electron in the Coulomb field.

The wave function of two electrons can be written as follows:

$$\Psi_{\beta\delta}^{JM}(\mathbf{x}_1, \mathbf{x}_2) = \frac{1}{\sqrt{2}}(\psi_{\beta\delta}^{JM}(\mathbf{x}_1, \mathbf{x}_2) - (-)^{j_\beta+j_\delta-J} \psi_{\delta\beta}^{JM}(\mathbf{x}_1, \mathbf{x}_2)). \quad (3.4)$$

The interaction energy of two electron holes can be obtained from equation

$$\epsilon_C = \int d\mathbf{x}_1 d\mathbf{x}_2 \Psi_{\beta\delta}^{JM\dagger}(\mathbf{x}_1, \mathbf{x}_2) \frac{e^2}{|\mathbf{x}_1 - \mathbf{x}_2|} \Psi_{\beta\delta}^{JM}(\mathbf{x}_1, \mathbf{x}_2). \quad (3.5)$$

The case of two holes with identical quantum numbers $\alpha = \beta$ and $m_\alpha \neq m_\beta$ requires special attention. The states $J = 2j \bmod(2)$ are symmetric over the $m_\alpha \leftrightarrow m_\beta$ permutations and do not exist. In the $J = 2j + 1 \bmod(2)$ case the states are anti-symmetric over the $m_\alpha \leftrightarrow m_\beta$ permutations, and the interaction energy should be divided by a factor of 2, since the superposition (3.3) changes the overall normalization of the two-electron wave function, as it follows from $C_{j m_1 j m_2}^{JM} = (-1)^{J-2j} C_{j m_2 j m_1}^{JM}$.

To simplify notations, we label the final states by indices α, γ and the initial ones by β, δ . The labels take values 1, 2 to indicate first and second electrons. There are two possibilities for the final state, $(\alpha, \gamma) = (1, 2)$ and $(2, 1)$, and two possibilities for the initial state, $(\beta, \delta) = (1, 2)$ and $(2, 1)$.

Equation (3.5) can be written as

$$\epsilon_C = K_{\beta\delta\beta\delta}^{JM} - (-)^{j_\beta+j_\delta-J} K_{\beta\delta\delta\beta}^{JM}, \quad (3.6)$$

where

$$K_{\alpha\gamma\beta\delta}^{JM} = \sum_{m_\alpha m_\gamma m_\beta m_\delta} C_{j_\alpha m_\alpha j_\gamma m_\gamma}^{JM} C_{j_\beta m_\beta j_\delta m_\delta}^{JM} K_{\alpha m_\alpha \gamma m_\gamma \beta m_\beta \delta m_\delta} \quad (3.7)$$

and

$$K_{\alpha m_\alpha \gamma m_\gamma \beta m_\beta \delta m_\delta} = \int d\mathbf{x}_1 d\mathbf{x}_2 [\Psi_{\alpha m_\alpha}^\dagger(\mathbf{x}_1) \Psi_{\beta m_\beta}(\mathbf{x}_1)] \frac{e^2}{|\mathbf{x}_1 - \mathbf{x}_2|} [\Psi_{\gamma m_\gamma}^\dagger(\mathbf{x}_2) \Psi_{\delta m_\delta}(\mathbf{x}_2)].$$

Further simplifications appear after the use of the expansion

$$\frac{1}{|\mathbf{x}_1 - \mathbf{x}_2|} = \sum_{lm} \frac{4\pi}{2l+1} \frac{r_{<}^l}{r_{>}^{l+1}} Y_{lm}(\mathbf{n}_1) Y_{lm}^*(\mathbf{n}_2), \quad (3.8)$$

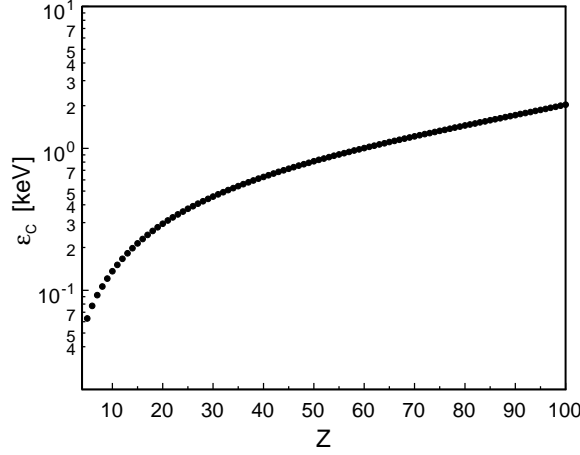


Figure 1: Coulomb interaction energy of two 1s electron holes versus nuclear charge Z .

where $r_< = \min(r_1, r_2)$, $r_> = \max(r_1, r_2)$, and \mathbf{n}_i are unit vectors toward \mathbf{x}_i .

The angular integrals are calculated with the use of equation

$$\int d\Omega_{\mathbf{n}} \Omega_{\alpha m_\alpha}^\dagger(\mathbf{n}) \Omega_{\beta m_\beta}(\mathbf{n}) Y_{lm}(\mathbf{n}) = C_{j_\beta m_\beta l m}^{j_\alpha m_\alpha} \mathcal{A}_{\alpha\beta}^l, \quad (3.9)$$

where $\Omega_{\alpha m_\alpha}(\mathbf{n})$ are spherical spinors [27],

$$\mathcal{A}_{\alpha\beta}^l = (-)^{1/2+j_\beta+l_\alpha+l} \sqrt{\frac{[l][l_\beta][j_\beta]}{4\pi}} C_{l_\beta 0 l 0}^{l_\alpha 0} \left\{ \begin{array}{ccc} 1/2 & l_\beta & j_\beta \\ l & j_\alpha & l_\alpha \end{array} \right\} \quad (3.10)$$

and $[x] = 2x + 1$.

The remaining two-dimensional integral over the radial variables,

$$K_{\alpha\gamma\beta\delta}^{JM} = e^2 \sum_l \frac{4\pi}{2l+1} C_{\alpha\beta\gamma\delta}^{Jl} \int r_1^2 dr_1 r_2^2 dr_2 \frac{r_<^l}{r_>^{l+1}} \mathcal{F}_{\alpha\beta}^l(r_1) \mathcal{F}_{\gamma\delta}^l(r_2), \quad (3.11)$$

can be calculated numerically or analytically using Maple. Here,

$$C_{\alpha\beta\gamma\delta}^{Jl} = (-)^{j_\gamma+j_\beta+J} \sqrt{[j_\alpha][j_\gamma]} \left\{ \begin{array}{ccc} l & j_\gamma & j_\delta \\ J & j_\beta & j_\alpha \end{array} \right\} \quad (3.12)$$

and

$$\mathcal{F}_{\alpha\beta}^l(r) = f_\alpha(r) f_\beta(r) \mathcal{A}_{\alpha\beta}^l + g_{\alpha'}(r) g_{\beta'}(r) \mathcal{A}_{\alpha'\beta'}^l, \quad (3.13)$$

where $\alpha = (njl)$, $\alpha' = (nj'l')$, and $l' = 2j - l$, and similarly for β .

In Fig. 1 we show the Coulomb interaction energy of two K holes as a function of the nuclear charge. As expected, the interaction energy increases approximately linearly with Z .

More accurate estimates of the interaction energy of electron holes can be obtained on the basis of the Breit potential, which takes into account relativistic effects $\sim (v/c)^2$. The accuracy of the present estimate, therefore, can be evaluated to be of order $(\alpha Z/n)^2$. For $Z = 60$ the expected error in the interaction energy of two K electron holes is about 20%. The accuracy is, of course, better for higher-shell atomic excitations.

3.2. Natural widths of excited electron shells

Decays of excited atoms are dominated by electric dipole transitions with the emission of X-ray photons and/or the emission of Auger electrons. Dipole decays are described in the literature in detail (see, e.g., [32]). For K vacancies, characteristic X-ray dipole emissions are dominant in atoms with $Z \gtrsim 35$. The dipole transition $2p \rightarrow 1s$ has a probability $\Gamma = 4 \times 10^{-7} Z^4$ eV (see, e.g., [32]). Since for a $(n+1)p \rightarrow ns$ decay, $\omega_{\alpha\beta} \sim 1/n^3$ and $d_{\alpha\beta} \sim n^2$, the corresponding width decreases as $\Gamma_{\alpha\beta} \sim 1/n^5$ for transitions from higher orbits. This effect is of interest, since the unitary limit of the width of the lepton number violating decay is inversely proportional to the width of the daughter atom (see Eq. (2.12)).

Auger transitions of excited atoms with one electron vacancy are well studied theoretically and experimentally (for a review see [29]). The width of a two-hole state $\alpha\beta$ is represented by

$$\Gamma_{\alpha\beta} = \Gamma_{\alpha} + \Gamma_{\beta} + \Gamma^*, \quad (3.14)$$

where Γ^* is the de-excitation width of daughter nucleus. Numerical values of the one-hole widths Γ_{α} are taken from Ref. [29]. These values cover the range $10 \leq Z \leq 92$ and one-electron vacancies from K to N7 shells ($1 \leq n \leq 4$). Equation (3.14) neglects the contributions from two-hole correlations.

3.3. Lepton number violating potential

We consider the $0\nu\text{ECEC}$ process assuming the standard form of the β -decay Hamiltonian

$$\mathcal{H}^{\beta}(x) = \frac{G_{\beta}}{\sqrt{2}} \bar{e}(x) \gamma^{\mu} (1 - \gamma_5) \nu_e(x) J_{\mu}(x) + \text{h.c.}, \quad (3.15)$$

where $G_{\beta} = G_F \cos \theta_C$ and θ_C is the Cabibbo angle. The field operators of the electron and electron neutrino are denoted as $e(x)$ and $\nu_e(x)$.

The left-handed electron neutrino $\nu_{eL}(x) = \frac{1-\gamma_5}{2} \nu_e(x)$ is a superposition of the left-handed projections of Majorana neutrinos χ_k with diagonal masses m_k :

$$\nu_{eL}(x) = \sum_{i=1}^3 U_{ek} \chi_{kL}(x). \quad (3.16)$$

Here, U is PMNS neutrino mixing matrix. Majorana neutrinos are truly neutral particles and obey $C \bar{\chi}_k^T = \xi_k \chi_k$, where $C = i\gamma_2 \gamma_0$ is the charge conjugation matrix and ξ_k is the phase factor.

The strangeness conserving charged hadron current has the form

$$J^{\mu}(x) = \bar{p}(x) \gamma^{\mu} (g_V - g_A \gamma_5) n(x), \quad (3.17)$$

where $n(x)$ and $p(x)$ are the field operators of the neutron and the proton, and the vector and axial-vector coupling constants are $g_V = 1$ and $g_A = 1.25$.

The potential of the $0\nu\text{ECEC}$ capture of two electrons with the total angular momentum J and projection M can be written as follows

$$\begin{aligned}
V_{\alpha\beta}(J_f^\pi) &= im_{\beta\beta} \left(\frac{G_\beta}{\sqrt{2}} \right)^2 \frac{1}{\sqrt{1 + \delta_{\alpha\beta}}} \sum_{m_\alpha m_\beta} C_{j_\alpha m_\alpha j_\beta m_\beta}^{JM} \int d\mathbf{x}_1 d\mathbf{x}_2 \quad (3.18) \\
&\times \Psi_{\alpha m_\alpha}^T(\mathbf{x}_1) C \gamma^\mu \gamma^\nu (1 - \gamma_5) \Psi_{\beta m_\beta}(\mathbf{x}_2) \int \frac{e^{-i\vec{q}\cdot(\mathbf{x}_1 - \mathbf{x}_2)} d\vec{q}}{2q_0 (2\pi)^3} \\
&\times \sum_n \left[\frac{\langle A, Z - 2 | J_\mu(\mathbf{x}_1) | n \rangle \langle n | J_\nu(\mathbf{x}_2) | A, Z \rangle}{q_0 + E_n - M_i - \varepsilon_\beta} \right. \\
&+ \left. \frac{\langle A, Z - 2 | J_\nu(\mathbf{x}_2) | n \rangle \langle n | J_\mu(\mathbf{x}_1) | A, Z \rangle}{q_0 + E_n - M_i - \varepsilon_\alpha} \right] - (\alpha \leftrightarrow \beta).
\end{aligned}$$

Here, $J_\mu(\mathbf{x})$ is the weak charged current in the Heisenberg representation. $|A, Z \rangle$ and $|A, Z - 2 \rangle$ are states of the initial and final nuclei. The sum is taken over all excitations of the intermediate nucleus ($A, Z - 1$). $\Psi_{\alpha m_\alpha}(\mathbf{x})$ is a wave function of the bound electron with quantum numbers $\alpha = (n_\alpha, j_\alpha, l_\alpha)$, projection of the total angular momentum m_α , and energy ε_α . The factor $1/\sqrt{1 + \delta_{\alpha\beta}}$ takes statistics of the captured electrons into account: $\delta_{\alpha\beta} = 1$ for the identical states and $\delta_{\alpha\beta} = 0$ otherwise.

In the derivation of $V_{\alpha\beta}(J^\pi)$, we neglected the small neutrino masses ($m_i \ll 10$ eV) in the neutrino potential, since the average exchange momentum in the process is large, $|\vec{q}| \simeq 200$ MeV/c. Further simplifications are as follows:

i) Non-relativistic impulse approximation for the nuclear current:

$$J^\mu(0, \mathbf{x}) = \sum_{n=1}^A \tau_n^- [g_V g^{\mu 0} + g_A (\sigma_k)_n g^{\mu k}] \delta(\mathbf{x} - \mathbf{x}_n). \quad (3.19)$$

ii) Closure approximation for the intermediate states: The excitation energies of the intermediate states $E_n - M_i$ are replaced by an average value $\langle E \rangle \approx 8$ MeV. In addition, we set $\varepsilon_{\alpha,\beta} \approx m$. The sum entering Eq. (3.18) is then calculated using completeness condition $\sum_n |n \rangle \langle n| = 1$.

iii) We restrict the calculation of the Majorana neutrino exchange potentials to the most favorable cases of even-even nuclei. Then the angular momentum of the initial nucleus is 0^+ and the angular momentum of the final (possibly excited) nucleus J^π must be balanced by the capture of the atomic electrons and the angular momentum of the atomic state.

The potential can finally be written as

$$V_{\alpha\beta}(J_f^\pi) = \frac{1}{4\pi} G_\beta^2 m_{\beta\beta} \frac{g_A^2}{R} \sqrt{2J_f + 1} \mathcal{M}_{\alpha\beta}(J_f^\pi). \quad (3.20)$$

Table 1: Combinations of the averaged upper and lower bi-spinor components of the electron wave functions entering the $0\nu\text{ECEC}$ potential for transitions $0_i^+ \rightarrow 0_f^\pm, 1_f^\pm$. Here, α, β are quantum numbers of electron hole states, and $F_{\alpha\beta}^{(\pm)}(r_n, r_m)$ and $H_{\alpha\beta}^{(\pm)}(r_n, r_m)$ are defined in Appendix B. If electron holes are in the same state, $\mathcal{A}_{\alpha\beta}$ should be divided by an additional factor $\sqrt{2}$.

Transitions	$\mathcal{A}_{\alpha\beta}$
$0^+ \rightarrow 0^+$	$\langle F_{\alpha\beta}^{(+)}(r_n, r_m) \rangle$
$0^+ \rightarrow 0^-$	$\langle H_{\alpha\beta}^{(+)}(r_n, r_m) \rangle$
$0^+ \rightarrow 1^+$	$\langle F_{\alpha\beta}^{(-)2}(r_n, r_m) \rangle^{1/2}$
$0^+ \rightarrow 1^-$	$\langle (H_{\alpha\beta}^{(-)}(r_n, r_m) - H_{\alpha\beta}^{(-)}(r_m, r_n))^2/4 \rangle^{1/2}$

In the case of a capture of $s_{1/2}$ and $p_{1/2}$ electrons and of a favorable case for the nuclear transitions $0^+ \rightarrow J_f^\pi = 0^\pm, 1^\pm$, the matrix elements $\mathcal{M}_{\alpha\beta}(J_f^\pi)$ are given in Appendix B.

The numerical analysis of the $0\nu\text{ECEC}$ transition is performed by factorizing the electron shell structure and the nuclear matrix element:

$$\mathcal{M}_{\alpha\beta}(J_f^\pi) \approx \mathcal{A}_{\alpha\beta} M^{0\nu}(J_f^\pi). \quad (3.21)$$

Here, $\mathcal{A}_{\alpha\beta}$ are lepton factors averaged over the nuclear volume. For low- J transitions, the lepton factors are given in Table 1.

The nuclear matrix elements of $0^+ \rightarrow 0^\pm$ transitions have the form

$$M^{0\nu}(0_f^+) = \langle 0_f^+ \parallel \sum_{nm} \tau_n^- \tau_m^- h(r_{nm}) [-\frac{g_V^2}{g_A^2} + (\boldsymbol{\sigma}_n \cdot \boldsymbol{\sigma}_m)] \parallel 0_i^+ \rangle, \quad (3.22)$$

$$\begin{aligned} M^{0\nu}(0_f^-) &= \langle 0_f^- \parallel \sum_{nm} \tau_n^- \tau_m^- h(r_{nm}) (\hat{\mathbf{r}}_n - \hat{\mathbf{r}}_m) \\ &\times [\frac{g_V}{g_A} (\boldsymbol{\sigma}_n - \boldsymbol{\sigma}_m) - i(\boldsymbol{\sigma}_n \times \boldsymbol{\sigma}_m)] \parallel 0_i^+ \rangle, \end{aligned} \quad (3.23)$$

where

$$h(r_{nm}) = \frac{2}{\pi} R \int_0^\infty j_0(qr_{nm}) \frac{q_0}{q_0 + \langle E \rangle - m} dq. \quad (3.24)$$

We note that the nuclear matrix element $M^{0\nu}(0_f^+)$ also appears in the calculation of the $0\nu\beta\beta$ -decay process [3].

For the transition $0^+ \rightarrow 1^\pm$ the lepton parts and the nuclear matrix elements are evaluated as discussed in Appendix A. We note that $\mathcal{A}_{\alpha\beta}$ vanishes for $0^+ \rightarrow 1^\pm$ transitions whenever the two electrons are captured from states with the same quantum numbers (njl) for $j = 1/2$. This is the reason, why e.g. the transition ${}_{68}^{162}\text{Er}(0^+) \rightarrow {}_{66}^{162}\text{Dy}^{**}(1^+, E_{\text{nucl}}^x = 1745.72 \text{ keV})$ is excluded from the analysis. If electrons are captured from different states, e.g., two $s_{1/2}$ electrons from different shells ($n_\alpha \neq n_\beta$) or from $s_{1/2}$ and $p_{1/2}$ states, the transition $0^+ \rightarrow 1^\pm$ is allowed and is considered in our analysis.

The dominant combinations of upper and lower component of bi-spinors, which enter the lepton part of the matrix elements after the factorization, are listed in

Table 1. The definition of functions $F_{\alpha\beta}^{(\pm)}(r_n, r_m)$ and $H_{\alpha\beta}^{(\pm)}(r_n, r_m)$ can be found in Appendix B. The decay rates of other transitions are estimated roughly with

$$2\pi\sqrt{2}\mathcal{A}_{\alpha\beta} \sim \sqrt{\langle f_\alpha^2 + g_\alpha^2 \rangle \langle f_\beta^2 + g_\beta^2 \rangle}. \quad (3.25)$$

The parity non-conservation in the weak interactions allows for instance transitions $0_i^+ \rightarrow 0_f^-, 1_f^-$ accompanied by capture of two S -wave or two P -wave electrons.

3.4. Likely resonant $0\nu ECEC$ transitions

We have considered all the nuclei and their excited states registered in the database of the Brookhaven National Laboratory [33] in August 2010, as well as all the combinatorial possibilities associated with the capture of two electrons. The selection criteria are as follows:

- i) The excitation energies are usually known with precision much higher than the atomic ground-state masses. We selected those pairs, where degeneracy occurs within the bounds given by a three standard deviation error of the ground-state mass measurements.
- ii) The unitary limit for the normalized half-life is less than 10^{27} years.

The half-lives are calculated using the formula

$$T_{1/2} = \frac{\ln 2}{\Gamma_1}, \quad (3.26)$$

where Γ_1 is given by Eq. (2.10).

Tables 2, 3, and 4 present the results of the selection over stable parent isotopes. We show the natural abundances NA, the spin-parity of the final nucleus J_f^π , the excitation energy of the final nucleus $E_{\text{nucl}}^x = M_{A,Z-2}^* - M_{A,Z-2}$, and the total mass difference $M_{A,Z-2}^{**} - M_{A,Z}$. The two errors indicate the errors of the ground-state mass measurements. Shown are as well the quantum numbers of the two hole states α and β in the electron shell, the energy of the holes (not including the electron rest mass), the Coulomb interaction energies of the holes ϵ_C , and the decay widths $\Gamma_{\alpha\beta}$. The last two columns show the minimum and maximum normalized $0\nu ECEC$ half-lives.

Tables 2, 3, and 4 list all, but no more than 5 transitions with the lowest quantum numbers of electron holes for each pair of the elements. If the spin is not fully determined, we took its lowest suggested value.

Rigorous calculations of the nuclear matrix elements (NME) based on the structure of nuclear states have not yet been performed. The objective here is to first select promising pairs of nuclei on the basis of rough estimates of the matrix elements, as these won't significantly change the global picture. The half-lives are normalized to the nuclear matrix element of $\mathcal{M}^{0\nu}(0_f^+) = 6$, which roughly corresponds to the maximum evaluated value of NMEs for medium-heavy nuclei [5]. Transitions to excited states are suppressed due to dissimilarity of the nuclear wave functions [34, 35].

Table 2: Likely resonant 0ν ECEC transitions. The list contains only those initial and final atoms, which are potentially degenerate at the level of a 3σ experimental error, and for which the unitary limit of the half-lives $\tilde{T}_{1/2}^{\min}$ is below 10^{27} years. The first column shows the natural abundances (NA in %) of the parent nuclei. In column 3 the spin and parity of the excited final nuclei (or their suggested values in parentheses or, if unknown, their assumed values in square brackets) are listed. Column 4 shows the excitation energies of the final nuclei with their present experimental errors. Column 5 lists the total mass differences, including the hole energies of the final nuclei, where the first error indicates the experimental uncertainty of the parent ground-state mass and the second the one of the daughter. The quantum numbers of the electron holes in the next two columns are $(n2jl)$, which are the principal quantum number, twice the total angular momentum, and the orbital angular momentum. Columns 8, 9, and 10 list the hole energies and the Coulomb interaction energies. Column 11 shows the widths of the excited electron shells. The last two columns show the minimum and maximum half-lives of the 0ν ECEC transitions (in years). Masses, energies and widths are given in keV.

NA	Transition	J_f^π	$M_{A,Z-2}^* - M_{A,Z-2}$	$M_{A,Z-2}^{**} - M_{A,Z}$	$(n2jl)_\alpha$	$(n2jl)_\beta$	ϵ_α^*	ϵ_β^*	ϵ_C	$\Gamma_{\alpha\beta}$	$\tilde{T}_{1/2}^{\min}$	$\tilde{T}_{1/2}^{\max}$
5.52%	${}^{96}_{44}\text{Ru} \rightarrow {}^{96}_{42}\text{Mo}^{**}$	0^+	2742 ± 1	$24.1 \pm 7.9 \pm 1.9$	310	410	0.50	0.06	0.02	9.5×10^{-3}	3×10^{26}	9×10^{33}
				$23.7 \pm 7.9 \pm 1.9$	410	410	0.06	0.06	0.01	6.4×10^{-3}	1×10^{27}	6×10^{34}
1.25%	${}^{106}_{48}\text{Cd} \rightarrow {}^{106}_{46}\text{Pd}^{**}$	$[0^+]$	2737 ± 1	$16.5 \pm 5.9 \pm 4.1$	110	110	24.35	24.35	0.74	1.3×10^{-2}	3×10^{23}	2×10^{30}
				$-4.8 \pm 5.9 \pm 4.1$	110	210	24.35	3.60	0.23	1.0×10^{-2}	9×10^{23}	3×10^{30}
				$-5.1 \pm 5.9 \pm 4.1$	110	211	24.35	3.33	0.21	8.5×10^{-3}	1×10^{26}	5×10^{32}
				$-7.9 \pm 5.9 \pm 4.1$	110	310	24.35	0.67	0.07	1.4×10^{-2}	4×10^{24}	9×10^{30}
				$-8.5 \pm 5.9 \pm 4.1$	110	410	24.35	0.09	0.02	1.1×10^{-2}	7×10^{24}	3×10^{31}
0.095%	${}^{124}_{54}\text{Xe} \rightarrow {}^{124}_{52}\text{Te}^{**}$	$[0^+]$	2853.2 ± 0.6	$-1.2 \pm 1.8 \pm 1.5$	210	210	4.94	4.94	0.16	4.4×10^{-3}	2×10^{24}	3×10^{30}
				$-1.6 \pm 1.8 \pm 1.5$	210	211	4.94	4.61	0.16	5.0×10^{-3}	2×10^{26}	2×10^{32}
				$-5.2 \pm 1.8 \pm 1.5$	210	310	4.94	1.01	0.08	1.2×10^{-2}	9×10^{24}	8×10^{30}
				$-5.4 \pm 1.8 \pm 1.5$	210	311	4.94	0.87	0.06	5.4×10^{-3}	5×10^{26}	2×10^{33}
				$-6.1 \pm 1.8 \pm 1.5$	210	410	4.94	0.17	0.02	4.6×10^{-3}	8×10^{24}	7×10^{31}
0.185%	${}^{136}_{58}\text{Ce} \rightarrow {}^{136}_{56}\text{Ba}^{**}$	0^+	2315.32 ± 0.07	$-27.5 \pm 13.3 \pm 0.4$	110	110	37.44	37.44	0.93	2.6×10^{-2}	1×10^{23}	7×10^{29}
0.185%	${}^{136}_{58}\text{Ce} \rightarrow {}^{136}_{56}\text{Ba}^{**}$	$[0^+]$	2349.5 ± 0.5	$6.7 \pm 13.3 \pm 0.4$	110	110	37.44	37.44	0.93	2.6×10^{-2}	1×10^{23}	2×10^{29}
				$-25.4 \pm 13.3 \pm 0.4$	110	210	37.44	5.99	0.30	1.5×10^{-2}	3×10^{23}	4×10^{30}
				$-25.8 \pm 13.3 \pm 0.4$	110	211	37.44	5.62	0.28	1.6×10^{-2}	3×10^{25}	4×10^{32}
				$-30.3 \pm 13.3 \pm 0.4$	110	310	37.44	1.29	0.09	2.4×10^{-2}	1×10^{24}	1×10^{31}
				$-30.5 \pm 13.3 \pm 0.4$	110	311	37.44	1.14	0.08	1.7×10^{-2}	1×10^{26}	2×10^{33}
0.185%	${}^{136}_{58}\text{Ce} \rightarrow {}^{136}_{56}\text{Ba}^{**}$	$(1^+, 2^+)$	2392.1 ± 0.6	$17.1 \pm 13.3 \pm 0.4$	110	210	37.44	5.99	0.21	1.5×10^{-2}	8×10^{22}	6×10^{29}
				$16.8 \pm 13.3 \pm 0.4$	110	211	37.44	5.62	0.29	1.6×10^{-2}	2×10^{24}	2×10^{31}
				$12.3 \pm 13.3 \pm 0.4$	110	310	37.44	1.29	0.07	2.4×10^{-2}	4×10^{23}	9×10^{29}
				$12.1 \pm 13.3 \pm 0.4$	110	311	37.44	1.14	0.08	1.7×10^{-2}	7×10^{24}	3×10^{31}
				$11.2 \pm 13.3 \pm 0.4$	110	410	37.44	0.25	0.03	1.6×10^{-2}	7×10^{23}	3×10^{30}

Table 3: Continued from Table 2.

NA	Transition	J_f^π	$M_{A,Z-2}^* - M_{A,Z-2}$	$M_{A,Z-2}^{**} - M_{A,Z}$	$(n2jl)_\alpha$	$(n2jl)_\beta$	ϵ_α^*	ϵ_β^*	ϵ_C	$\Gamma_{\alpha\beta}$	$T_{1/2}^{\min}$	$T_{1/2}^{\max}$
0.185%	$^{136}_{58}\text{Ce} \rightarrow ^{136}_{56}\text{Ba}^{**}$	$(1^+, 2^+)$	2399.87 ± 0.05	$24.9 \pm 13.3 \pm 0.4$	110	210	37.44	5.99	0.21	1.5×10^{-2}	8×10^{22}	1×10^{30}
				$24.6 \pm 13.3 \pm 0.4$	110	211	37.44	5.62	0.29	1.6×10^{-2}	2×10^{24}	3×10^{31}
				$20.0 \pm 13.3 \pm 0.4$	110	310	37.44	1.29	0.07	2.4×10^{-2}	4×10^{23}	2×10^{30}
				$19.9 \pm 13.3 \pm 0.4$	110	311	37.44	1.14	0.08	1.7×10^{-2}	7×10^{24}	5×10^{31}
				$18.9 \pm 13.3 \pm 0.4$	110	410	37.44	0.25	0.03	1.6×10^{-2}	7×10^{23}	5×10^{30}
0.20%	$^{152}_{64}\text{Gd} \rightarrow ^{152}_{62}\text{Sm}^*$	0^+	0	$-0.8 \pm 2.5 \pm 2.5$	110	210	46.83	7.74	0.34	2.3×10^{-2}	2×10^{23}	8×10^{26}
				$-1.3 \pm 2.5 \pm 2.5$	110	211	46.83	7.31	0.32	2.3×10^{-2}	2×10^{25}	2×10^{29}
				$-7.1 \pm 2.5 \pm 2.5$	110	310	46.83	1.72	0.11	3.2×10^{-2}	7×10^{23}	1×10^{29}
				$-7.3 \pm 2.5 \pm 2.5$	110	311	46.83	1.54	0.10	2.5×10^{-2}	5×10^{25}	2×10^{31}
				$-8.5 \pm 2.5 \pm 2.5$	110	410	46.83	0.35	0.04	2.4×10^{-2}	1×10^{24}	6×10^{29}
0.06%	$^{156}_{66}\text{Dy} \rightarrow ^{156}_{64}\text{Gd}^{**}$	1^-	1946.375 ± 0.006	$-7.5 \pm 6.6 \pm 2.5$	110	211	50.24	7.93	0.34	2.6×10^{-2}	8×10^{23}	5×10^{29}
				$-14.0 \pm 6.6 \pm 2.5$	110	311	50.24	1.69	0.10	2.8×10^{-2}	2×10^{24}	3×10^{30}
				$-15.5 \pm 6.6 \pm 2.5$	110	411	50.24	0.29	0.03	2.8×10^{-2}	5×10^{24}	8×10^{30}
0.06%	$^{156}_{66}\text{Dy} \rightarrow ^{156}_{64}\text{Gd}^{**}$	0^-	1952.385 ± 0.007	$-1.1 \pm 6.6 \pm 2.5$	110	210	50.24	8.38	0.35	2.6×10^{-2}	2×10^{24}	6×10^{29}
				$-1.5 \pm 6.6 \pm 2.5$	110	211	50.24	7.93	0.34	2.6×10^{-2}	4×10^{25}	1×10^{31}
				$-7.8 \pm 6.6 \pm 2.5$	110	310	50.24	1.88	0.11	3.5×10^{-2}	9×10^{24}	3×10^{30}
				$-8.0 \pm 6.6 \pm 2.5$	110	311	50.24	1.69	0.10	2.8×10^{-2}	1×10^{26}	7×10^{31}
				$-9.4 \pm 6.6 \pm 2.5$	110	410	50.24	0.38	0.04	2.7×10^{-2}	2×10^{25}	1×10^{31}
0.06%	$^{156}_{66}\text{Dy} \rightarrow ^{156}_{64}\text{Gd}^{**}$	1^-	1962.037 ± 0.012	$8.1 \pm 6.6 \pm 2.5$	110	211	50.24	7.93	0.34	2.6×10^{-2}	8×10^{23}	5×10^{29}
				$1.6 \pm 6.6 \pm 2.5$	110	311	50.24	1.69	0.10	2.8×10^{-2}	2×10^{24}	6×10^{29}
				$0.2 \pm 6.6 \pm 2.5$	110	411	50.24	0.29	0.03	2.8×10^{-2}	5×10^{24}	1×10^{30}
0.06%	$^{156}_{66}\text{Dy} \rightarrow ^{156}_{64}\text{Gd}^{**}$	1^+	1965.950 ± 0.004	$12.4 \pm 6.6 \pm 2.5$	110	210	50.24	8.38	0.26	2.6×10^{-2}	4×10^{22}	4×10^{28}
				$12.0 \pm 6.6 \pm 2.5$	110	211	50.24	7.93	0.34	2.6×10^{-2}	8×10^{23}	8×10^{29}
				$5.7 \pm 6.6 \pm 2.5$	110	310	50.24	1.88	0.09	3.5×10^{-2}	2×10^{23}	4×10^{28}
				$5.6 \pm 6.6 \pm 2.5$	110	311	50.24	1.69	0.10	2.8×10^{-2}	2×10^{24}	9×10^{29}
				$4.2 \pm 6.6 \pm 2.5$	110	410	50.24	0.38	0.03	2.7×10^{-2}	3×10^{23}	1×10^{29}
0.06%	$^{156}_{66}\text{Dy} \rightarrow ^{156}_{64}\text{Gd}^{**}$	$[0^+]$	1970.2 ± 0.8	$16.7 \pm 6.6 \pm 2.5$	110	210	50.24	8.38	0.35	2.6×10^{-2}	1×10^{23}	2×10^{29}
				$16.3 \pm 6.6 \pm 2.5$	110	211	50.24	7.93	0.34	2.6×10^{-2}	1×10^{25}	2×10^{31}
				$10.0 \pm 6.6 \pm 2.5$	110	310	50.24	1.88	0.11	3.5×10^{-2}	6×10^{23}	3×10^{29}
				$9.8 \pm 6.6 \pm 2.5$	110	311	50.24	1.69	0.10	2.8×10^{-2}	4×10^{25}	3×10^{31}
				$8.4 \pm 6.6 \pm 2.5$	110	410	50.24	0.38	0.04	2.7×10^{-2}	1×10^{24}	7×10^{29}

Table 4: Continued from Table 3.

NA	Transition	J_f^π	$M_{A,Z-2}^* - M_{A,Z}$	$M_{A,Z-2}^{**} - M_{A,Z}$	$(n2jl)_\alpha$	$(n2jl)_\beta$	ϵ_α^*	ϵ_β^*	ϵ_C	$\Gamma_{\alpha\beta}$	$\overline{T}_{1/2}^{\min}$	$\overline{T}_{1/2}^{\max}$
0.06%	$^{156}_{66}\text{Dy} \rightarrow ^{156}_{64}\text{Gd}^{**}$	0^+	1988.5 ± 0.2	$-7.0 \pm 6.6 \pm 2.5$	210	210	8.38	8.38	0.21	7.6×10^{-3}	5×10^{23}	3×10^{30}
				$-7.4 \pm 6.6 \pm 2.5$	210	211	8.38	7.93	0.22	7.7×10^{-3}	2×10^{25}	2×10^{32}
				$-13.6 \pm 6.6 \pm 2.5$	210	310	8.38	1.88	0.10	1.7×10^{-2}	2×10^{24}	6×10^{30}
				$-13.8 \pm 6.6 \pm 2.5$	210	311	8.38	1.69	0.09	9.4×10^{-3}	8×10^{25}	8×10^{32}
				$-15.1 \pm 6.6 \pm 2.5$	210	410	8.38	0.38	0.03	8.7×10^{-3}	2×10^{24}	3×10^{31}
0.06%	$^{156}_{66}\text{Dy} \rightarrow ^{156}_{64}\text{Gd}^{**}$	1^+	2026.664 ± 0.006	$17.9 \pm 6.6 \pm 2.5$	310	311	1.88	1.69	0.07	1.8×10^{-2}	3×10^{25}	1×10^{32}
				$16.5 \pm 6.6 \pm 2.5$	310	410	1.88	0.38	0.02	1.8×10^{-2}	4×10^{24}	2×10^{31}
				$16.4 \pm 6.6 \pm 2.5$	310	411	1.88	0.29	0.03	1.8×10^{-2}	7×10^{25}	3×10^{32}
				$16.3 \pm 6.6 \pm 2.5$	311	410	1.69	0.38	0.03	1.0×10^{-2}	4×10^{25}	5×10^{32}
				$16.2 \pm 6.6 \pm 2.5$	311	411	1.69	0.29	0.02	1.1×10^{-2}	7×10^{26}	8×10^{33}
1.56%	$^{164}_{68}\text{Er} \rightarrow ^{164}_{66}\text{Dy}^*$	0^+	0	$-5.5 \pm 3.1 \pm 2.5$	210	210	9.05	9.05	0.22	8.6×10^{-3}	4×10^{23}	1×10^{30}
				$-5.9 \pm 3.1 \pm 2.5$	210	211	9.05	8.58	0.23	8.3×10^{-3}	2×10^{25}	5×10^{31}
				$-12.6 \pm 3.1 \pm 2.5$	210	310	9.05	2.05	0.11	1.8×10^{-2}	1×10^{24}	3×10^{30}
				$-12.8 \pm 3.1 \pm 2.5$	210	311	9.05	1.84	0.09	1.0×10^{-2}	6×10^{25}	4×10^{32}
				$-6.4 \pm 3.1 \pm 2.5$	211	211	8.58	8.58	0.27	8.0×10^{-3}	1×10^{26}	5×10^{32}
0.14%	$^{168}_{70}\text{Yb} \rightarrow ^{168}_{68}\text{Er}^{**}$	1^-	1358.898 ± 0.005	$3.9 \pm 4.4 \pm 2.5$	110	211	57.49	9.26	0.38	3.3×10^{-2}	4×10^{23}	7×10^{28}
				$-3.6 \pm 4.4 \pm 2.5$	110	311	57.49	2.01	0.11	3.5×10^{-2}	1×10^{24}	2×10^{29}
				$-5.3 \pm 4.4 \pm 2.5$	110	411	57.49	0.37	0.04	3.4×10^{-2}	3×10^{24}	5×10^{29}
0.14%	$^{168}_{70}\text{Yb} \rightarrow ^{168}_{68}\text{Er}^{**}$	0^+	1422.10 ± 0.03	$12.0 \pm 4.4 \pm 2.5$	210	310	9.75	2.21	0.11	1.8×10^{-2}	1×10^{24}	2×10^{30}
				$11.8 \pm 4.4 \pm 2.5$	210	311	9.75	2.01	0.10	1.1×10^{-2}	4×10^{25}	2×10^{32}
				$11.5 \pm 4.4 \pm 2.5$	211	310	9.26	2.21	0.10	1.8×10^{-2}	8×10^{25}	2×10^{32}
				$11.4 \pm 4.4 \pm 2.5$	211	311	9.26	2.01	0.13	1.1×10^{-2}	2×10^{26}	8×10^{32}
				$9.7 \pm 4.4 \pm 2.5$	211	410	9.26	0.45	0.04	1.0×10^{-2}	1×10^{26}	5×10^{32}
0.13%	$^{180}_{74}\text{W} \rightarrow ^{180}_{72}\text{Hf}^*$	0^+	0	$-12.0 \pm 3.9 \pm 2.1$	110	110	65.35	65.35	1.26	7.2×10^{-2}	3×10^{22}	4×10^{27}
0.02%	$^{184}_{76}\text{Os} \rightarrow ^{184}_{74}\text{W}^{**}$	$(0)^+$	1322.152 ± 0.022	$11.3 \pm 1.3 \pm 0.9$	110	110	69.53	69.53	1.31	8.0×10^{-2}	7×10^{26}	2×10^{27}
0.014%	$^{190}_{78}\text{Pt} \rightarrow ^{190}_{76}\text{Os}^{**}$	$(1, 2, 3)^+$	1382.4 ± 0.2	$15.6 \pm 5.7 \pm 1.5$	210	310	12.97	3.05	0.13	2.2×10^{-2}	3×10^{23}	8×10^{29}
				$15.4 \pm 5.7 \pm 1.5$	210	311	12.97	2.79	0.12	1.6×10^{-2}	1×10^{25}	6×10^{31}
				$13.2 \pm 5.7 \pm 1.5$	210	410	12.97	0.65	0.05	1.5×10^{-2}	5×10^{23}	2×10^{30}
				$3.2 \pm 5.7 \pm 1.5$	310	410	3.05	0.65	0.04	2.2×10^{-2}	3×10^{24}	1×10^{30}
				$0.8 \pm 5.7 \pm 1.5$	410	410	0.65	0.65	0.03	1.5×10^{-2}	9×10^{24}	5×10^{30}

The half-lives are further normalized to an effective neutrino mass of $|m_{\beta\beta}| = 1$ eV. The normalized half-lives listed in Tables 2, 3, and 4 are then given as

$$\tilde{T}_{1/2} = T_{1/2} \left| \frac{m_{\beta\beta}}{1 \text{ eV}} \right|^2 \left| \frac{M^{0\nu}(J_f^\pi)}{\mathcal{M}^{0\nu}(0_f^+)} \right|^2. \quad (3.27)$$

The unitary limit, i.e. the minimum value of $\tilde{T}_{1/2}$ (denoted as $\tilde{T}_{1/2}^{\min}$) is given for a full mass degeneracy of initial and final atoms. The maximum value $\tilde{T}_{1/2}^{\max}$ is obtained by substituting in Eq. (2.10) the mass difference squared

$$\Delta M^2 = (M_{A,Z-2}^{**} - M_{A,Z})^2 + \Delta M_{\text{expt}}^2, \quad (3.28)$$

where the last term accounts for the experimental errors of the masses and the nuclear excited state:

$$\Delta M_{\text{expt}}^2 = \delta M_{A,Z-2}^2 + \delta M_{A,Z}^2 + \delta E_{\text{nucl}}^{x2}. \quad (3.29)$$

The atomic mass differences are occasionally known with higher precision than the individual masses. The normalized half-lives, however, should stay between the two bounds given by $\tilde{T}_{1/2}^{\min}$ and $\tilde{T}_{1/2}^{\max}$.

There are some other $0\nu\text{ECEC}$ transitions, which may deserve an extra comment:

- ${}^{78}_{36}\text{Kr}(0^+) \rightarrow {}^{78}_{34}\text{Se}^{**}$

This transition has a decay ECEC Q-value of 2867.5 keV and appears in the list of likely resonant transitions in Ref. [15]. The final nucleus has an excited state at 2864 keV, however, with unknown spin and parity. The state, however, γ decays by 100% into the 3^+ state at 1054 keV state, which essentially excludes a spin $J = 0, 1$ assignment for the 2864 keV state. This transition is excluded from our list.

- ${}^{96}_{44}\text{Ru}(0^+) \rightarrow {}^{96}_{42}\text{Mo}^{**}$

A mass degeneracy of initial and final atoms could occur for this transition by considering the excitation of final nucleus with 2712.68 keV. The angular momentum and parity of this excited state are not known yet. However, it decays to state with $J^\pi = 5^+/6^+$, which excludes a spin $J = 0, 1$ assignment for this state. Therefore, this transition is excluded from the list as well.

- ${}^{106}_{48}\text{Cd}(0^+) \rightarrow {}^{106}_{46}\text{Pd}^{**}$

This transition might be a resonant transition in the case the palladium isotope remains in an excited nuclear state at 2717.59 keV. However, the state γ decays by 100% into the 3^+ state at 1557.68 keV state, which again excludes a possibility of $J = 0, 1$ for this state.

- ${}^{112}_{50}\text{Sn}(0^+) \rightarrow {}^{112}_{48}\text{Cd}^{**}(0^+)$

The transition through the excited level at 1871 keV (0^+) has been widely discussed in the literature [15]. As already noted earlier, the masses and thereby

the Q-value for the ground-state ECEC decay have been re-measured with high accuracy to $Q = 1919.82$ keV [16]. A double K-shell excitation of the final atom requires about 55 keV, thereby leaving not enough energy to excite the 1871 keV state. This transition is therefore not considered anymore in Tables 2, 3, and 4.

- ${}_{56}^{130}\text{Ba} \rightarrow {}_{54}^{130}\text{Xe}^{**}$

The excitation level of 2544.43 ± 0.08 keV with unknown spin-parity gives a quite low half-life assuming $J^\pi = 0^\pm$ and a double capture of K electrons. If higher electron levels are involved, the degeneracy gets broken. The excited ${}_{54}^{130}\text{Xe}^*$ level decays by 100 units into the 2^+ state at 536 keV and by 10 units to the ground state. The strong ground state mode excludes a 0^+ assignment. Possible assignments are $J \geq 1$. Two K electrons have $J = 0$, so such options are forbidden by the conservation of angular momentum.

There is a possibility of a resonant enhancement of the $0\nu\text{ECEC}$ of ${}^{130}\text{Ba}$ by considering a nuclear excitation of ${}^{130}\text{Xe}$ at 2608.43 keV or 2622.32 keV. The angular momentum and parity of these states are not clarified yet. Unfortunately, a favored possibility of 0^+ excited state is excluded, because the γ -decay of these levels feed into a 4^+ state. These transitions have not been considered in Tables 2 - 4.

- ${}_{68}^{162}\text{Er}(0^+) \rightarrow {}_{66}^{162}\text{Dy}^{**}(1^+)$

The decay of ${}_{68}^{162}\text{Er}$ (ECEC Q-value 1845 keV) with the excitation of the 1745.72 ($J_f^\pi = 1^+$) keV state in ${}_{66}^{162}\text{Dy}$ is a good candidate as far as energy matching is concerned. A double K-shell capture requires about 110 keV, however, the transition to a 1^+ final state is strictly Pauli-forbidden.

- ${}_{76}^{184}\text{Os} \rightarrow {}_{74}^{184}\text{W}^{**}(0)^+$

In the transition to the 1322 keV excited state of ${}_{74}^{184}\text{W}$, the mass difference exceeds three standard deviations. Accordingly, we do not expect a complete degeneracy. However, the minimum half-life estimated for three standard deviations in the direction of a smaller mass difference is less than 10^{27} years. This decay is included in the tables. Shown in place of the unitary limit is the minimum half-life found in this way.

All systems in Tables 2, 3, and 4 start out from stable parent nuclei. We also investigated unstable and radioactive candidate nuclei, in particular those with rather long half-lives. However, none of them was found to be of practical use. Even if those nuclei could be produced in reasonably large quantities, activity levels would be prohibitive.

3.5. Likely resonant $0\nu\text{EPEP}$ transitions

The selection criteria have also been applied to the neutrinoless double electron production (EPEP), where the two electrons are placed into a bound state above the occupied electron shell of the final atom (see Eq. (1.5)), and where the simultaneous nuclear excitation provides the mass degeneracy. Clearly, this process is expected to

be rather unlikely, as it requires that a Q -value be extremely fine-tuned to a nuclear excitation. If such a case existed, the two electrons would be placed into any of the upper most non-occupied electron shells of the final atom, whereby the width of the resonant decay would then be controlled by the width of the excited nucleus. The atomic de-excitation width would be comparatively small, or even zero in the case the electrons occupied the atomic ground state.

As an instructive test, we analyze the 0ν EPEP transition of $^{148}_{60}\text{Nd}(0^+)$ (isotopic abundance: 5.8%) to the 1920.97 keV excited 0^+ state in $^{148}_{62}\text{Sm}$. In this case the difference of the atomic masses is $M_{A,Z+2}^* - M_{A,Z} = 7.2 \pm 2.8 \pm 2.4$ keV. The ground-state configuration of the $^{148}_{62}\text{Sm}$ daughter atom is $4f^66s^2$, whereas the one of $^{148}_{60}\text{Nd}$ is $4f^46s^2$. The 0ν EPEP transition to the $4f^66s^2$ ground state of $^{148}_{62}\text{Sm}$ is disallowed by angular momentum, as it requires the production of two electrons with $l = 3$. The most favored 0ν EPEP transition would be an atomic excitation of $^{148}_{62}\text{Sm}$, whereby the two electrons were placed into the $7s$ shell. The atomic width is small, and we estimate that the unitary limit assuming the nuclear half-life of 0.1 ps. The calculated shortest half-life would be above 10^{27} y.

3.6. Data analysis of candidate transitions

Tables 2, 3, and 4 also give a list of decays in which the unitary limit for the half-life of the atom turns out to be low, because the low probability of capture of electrons from higher orbits is compensated by a low probability of de-excitation of the electron shell. The probability of finding degeneracy with an accuracy comparable to the de-excitation width, of course, decreases with the de-excitation width. The number of such transitions, however, is sufficiently large, so it makes sense to evaluate the chances of detecting degeneracy with improving the accuracy of the measurements, taking into account all the states. We restricted ourselves to the capture of electrons from the orbits with principal quantum number no higher than 4. Higher states may also participate in the decays, however, we have not considered them, because data on the de-excitation widths of electron shells with principal quantum number higher than 4 are not available.

The objective of the analysis of this subsection is to estimate a priori probability of finding in future experiments an atom with a half-life of less than some fixed value.

The analysis is made by considering all transitions listed in Tables 2, 3, and 4, as well as the transitions associated with the capture of electrons from higher orbits, that passed our filters, but were not included in Tables 2, 3, and 4, as long as we list not more than 5 transitions for each pair of the nuclei, associated with the electron capture from lowest orbits.

In the spirit of the Bayesian method, the mass difference between initial and final atoms is regarded as a random variable. We assume further that this value, η , is normally distributed around the current experimental value $M_{A,Z-2}^{**} - M_{A,Z}$ with a dispersion determined by the current experimental error ΔM_{expt} . Future measurement of the mass difference between pairs of atoms with an accuracy of $\Delta\mu$ is consistent with the hypothesis of the degeneracy of atoms with a probability

$$w(\Delta\mu) = \int_{-\Delta\mu}^{\Delta\mu} \frac{d\eta}{\sqrt{2\pi}\Delta M_{\text{expt}}} \exp\left(-\frac{(\eta - M_{A,Z-2}^{**} + M_{A,Z})^2}{2\Delta M_{\text{expt}}^2}\right). \quad (3.30)$$

Suppose a measurement gives $\eta = 0$ with the accuracy of $\Delta\mu \sim \Gamma_{\alpha\beta}$. For the normal distribution of η , in the likely resonant case $(M_{A,Z-2}^{**} - M_{A,Z})^2 \sim \Delta M_{\text{expt}}^2$, and for a small $\Gamma_{\alpha\beta}$, the probability of finding the complete degeneracy and thereby of getting the unitary limit equals $w(\Delta\mu) \sim \Gamma_{\alpha\beta}/\Delta M_{\text{expt}}$, in agreement with naive expectations.

The half-live $\tilde{T}_{1/2}$ of a particular transition may be written as

$$\tilde{T}_{1/2} = \tilde{T}_{1/2}^{\min} \frac{\Delta M^2 + \Gamma_{\alpha\beta}^2/4}{\Gamma_{\alpha\beta}^2/4}, \quad (3.31)$$

where ΔM is defined in Eq. (3.28). To have a decay time less than $\tilde{T}_{1/2}$, it is sufficient to claim experimentally $\eta = 0$ with an accuracy better than

$$\Delta\mu(\tilde{T}_{1/2}) = \frac{\Gamma_{\alpha\beta}}{2} \left(\frac{\tilde{T}_{1/2}}{\tilde{T}_{1/2}^{\min}} - 1 \right)^{1/2}. \quad (3.32)$$

The value of $\Delta\mu(\tilde{T}_{1/2})$ is the maximum error, at which the decay time is shorter than $\tilde{T}_{1/2}$.

The number of transitions, n_T , to be found with half-lives below $\tilde{T}_{1/2}$ can be estimated by summing up the Gaussian probabilities

$$n_T = \sum w(\Delta\mu(\tilde{T}_{1/2})) \equiv \sum \left(\frac{1}{2} \operatorname{erf} \left(\frac{M_{A,Z-2}^{**} - M_{A,Z} + \Delta\mu(\tilde{T}_{1/2})}{\sqrt{2}\Delta M_{\text{expt}}} \right) - \frac{1}{2} \operatorname{erf} \left(\frac{M_{A,Z-2}^{**} - M_{A,Z} - \Delta\mu(\tilde{T}_{1/2})}{\sqrt{2}\Delta M_{\text{expt}}} \right) \right). \quad (3.33)$$

The sum runs over the transitions with $\tilde{T}_{1/2}^{\min} < \tilde{T}_{1/2}$, listed in Tables 2, 3, and 4.

The results are shown in Fig. 2. There are 2 chances out of 100 to find the transition with a normalized half-life below 10^{24} years, 13 chances out of 100 to find the transition with a normalized half-life below 10^{25} years, 45 chances out of 100 to find the transition with a normalized half-life below 10^{26} years. We also expect ~ 2 transitions with $\tilde{T}_{1/2} < 10^{27}$ years.

Under the specified conditions, the chance of finding after precise mass measurements a $0\nu\text{ECEC}$ decay more sensitive to the Majorana neutrino mass than the benchmark ^{76}Ge neutrinoless $\beta^-\beta^-$ decay is close to $\sim 1 : 25$. The experimental search for the $0\nu\text{ECEC}$ decay is thus expected to be more complicated. The background conditions in the $0\nu\text{ECEC}$ decay are, however, very favorable (see Sect. 4).

Here, all the transitions are treated as statistically independent. For most of the transitions in Tables 2, 3, and 4, this condition is certainly not satisfied, because for the same atom, together with the capture of electrons from the lower shells, one generally has captures of electrons from the high-lying levels. One precise measurement of the atomic mass difference either excludes the entire group, or allows all (or nearly all) transitions. Breit-Wigner resonances corresponding to the different electron states have a typical width of less than ~ 10 eV. In our case, such resonances do

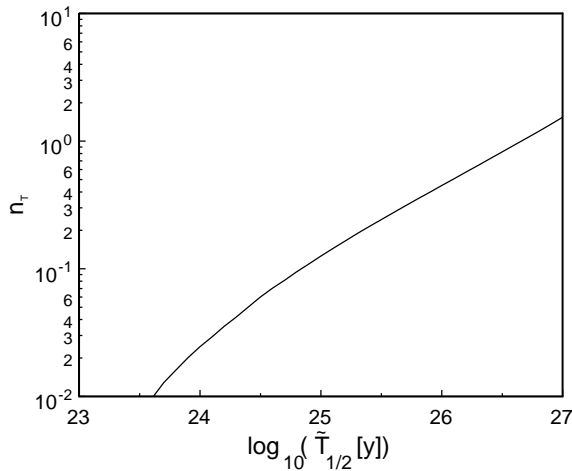


Figure 2: Expected number of transitions with a normalized half-life below $\tilde{T}_{1/2}$, provided accurate measurements are made to determine the mass difference between pairs of atoms listed in Tables 2, 3, and 4.

not overlap and are summed up additively. An increase in the decay probability is equivalent to registering an excess of events. The number of events calculated from Eq. (3.33) takes into account this effect. Although the list of transitions splits into the correlated groups, the statistically independent count of the expected decays is justified. While the correlations do not influence n_T , they obviously increase the dispersion of n_T .

The accuracy of 10 eV in the measurement of atomic masses will be achievable in the near future [18]. The electron binding energy depends on the local physical and chemical environment. An interesting question is whether and how to manage the atomic structure in such a way as to artificially implement the degeneracy of the atoms and create conditions for the resonant enhancement.

The effects of finite density and temperature on the profile of the atomic spectral lines were studied theoretically and experimentally starting from the 1930's. To give an idea of the magnitude of the effect, we give some numbers. In ionized atoms of He I, photon energy emitted in the transition between the levels $3p$ and $2s$ at a density of 10^{18}cm^{-3} and temperature $T = 5000$ K changes by about 10 meV (see, e.g., [39], Sect. 39). In metals, when the temperature varies from 100 K to room temperature, levels $1s$ in Li, ..., $4p$ in Rb get shifted by several tens of meV [40]. These values are 2-3 orders of magnitude smaller than the width of electron holes in the atoms, so the influence of the environment in such a case is not sufficient and, apparently, is not of interest.

The chemical composition of matter also may influence the binding energies. In comparison with the free atoms, the energy of atomic electrons in metals gets shifted by a few eV [41]. The total effect on the mass difference of atoms connected by double-electron capture can reach $\sim Z$ eV, which exceeds the typical natural width

~ 10 eV of the electron holes in medium-heavy and heavy atoms. The effect of chemical composition deserves more detailed analysis.

4. Experimental signatures of 0ν ECEC decay

Double beta ($\beta\beta$) decay of any variant is a process with a notoriously small probability, where typical decay times are at least of the order 10^{19} y in the most fortuitous cases. These values pertain to the ordinary cases, where 2ν are involved. For the more relevant neutrinoless decays, half-lives are expected to be even longer by at least another 3 to 4 orders of magnitude owing to the fact that the rate scales with the square of the mass of the Majorana neutrino. To detect these extremely rare processes in a real experiment, requires an enormous effort in background reduction. There are two typical and rather different sources of backgrounds one has to deal with, cosmic ray interactions (including cosmogenically produced radio-isotopes) and the ambient radioactivity. Even in underground laboratories like the ones at Gran Sasso or at Modane, which provide a natural 3100 meter, resp. 4800 meter water equivalent shielding against cosmic rays, an experimental setup for $\beta\beta$ decay measurements still requires a massive active and passive shielding before any attempt can be made to venture into life-times of the order of 10^{24} y and above [6, 36, 37]. Typical probe masses are then still several tens or hundreds of kilograms.

Double beta decay experiments so far have focused almost entirely on the $\beta^-\beta^-$ -decay variant and little attention has been devoted to a possible decay from the β^+ direction. Indeed, the $\beta^-\beta^-$ -decay comes with a rather simple and comparatively easy to detect signature: in the $2\nu\beta^-\beta^-$ -decay the summed energy spectrum of the two electrons carries the signature of a 4-body decay, whereas a single, mono-energetic peak at the endpoint energy signals the neutrinoless decay. However, because the summed electron energy of the $2\nu\beta^-\beta^-$ -decay extends all the way to the endpoint region, any background in this region becomes a serious issue. The spectral resolution of the experiment is then most critical parameter, which determines the sensitivity of the experiment.

The signatures of a decay from the β^+ direction are rather different. We will not enter into a detailed discussion about $\beta^+\beta^+$ or β^+ EC decay, as there is an extra energy penalty of $2m_e c^2$ to be paid for each β^+ production on top of a rather disadvantageous β^+ phase-space factor and final-state Coulomb repulsion.

We focus on the ECEC process instead. In comparison with the $\beta^-\beta^-$ -decay, prospects for measuring the ECEC-decay looked at the beginning rather pessimistic. Generally low isotopic abundances add to the difficulties. At present, there is only one experiment, which has advanced quite significantly. This is the TGV experiment [38] in the Modane underground laboratory looking for the ECEC decay of ^{106}Cd through the identification of ≈ 20 keV X-rays. The collaboration has already reached an impressive lower limit for the 2ν ECEC decay of $T_{1/2} > 2.6 \cdot 10^{20}$ y (90%). On the other hand, the neutrinoless ECEC decay usually requires an extra photon, which must carry away the excess energy given by the Q-value of the transition (which is about 2.7 MeV in the ^{106}Cd case). This causes an extra suppression and the expected half-life is above 10^{30} years for $m_{\beta\beta} = 1$ eV by referring to a calculation

performed for ^{112}Sn [10].

The ECEC process discussed in this paper brings in a new aspect, which could be rather advantageous as far as the experimental conditions are concerned. If Nature provides us with a mass degeneracy, as discussed in this paper, the decay proceeds through a narrow resonance and the rate increases dramatically giving half-lives which are competitive to the neutrinoless $\beta^-\beta^-$ decays. On top of this, there are several additional advantages. The de-excitation of the final excited nucleus proceeds in most cases through a cascade of easy to detect γ rays. A two- or even higher-fold coincidence setup can cut down any background rate right from the beginning, thereby requiring significantly less active or passive shielding. For instance in the ^{136}Ba case, the 2315 keV level would go through the cascade $2315(0^+) \rightarrow 818(2^+) \rightarrow \text{g.s.}(0^+)$ (2γ rays) and in the ^{156}Gd case, the 1952 keV level would de-excite as $1952(0^-) \rightarrow 1242(1^-) \rightarrow 89(2^+) \rightarrow \text{g.s.}(0^+)$ (3γ rays). A mere detection of these γ rays would already signal the ECEC decay beyond any doubt, as there are no other background processes feeding those particular nuclear levels. Further, the lepton number conserving ECEC decay with two neutrinos,

$$(A, Z) + e_b^- + e_b^- \rightarrow (A, Z - 2)^{**} + \nu_e + \nu_e, \quad (4.34)$$

is strongly suppressed due to the almost vanishing phase space. Note that the 2ν phase space has a dependence of Q^5 , with Q being the remaining excess energy. For a Q -value in the low MeV region the half-life of the $2\nu\text{ECEC}$ is about 10^{22} years [42]. For the considered ECEC transitions in (4.34) the Q -value is assumed to be below a keV, which already gives a suppression by at least another 15 orders of magnitude. Thus, the signature for a $0\nu\text{ECEC}$ resonant transition would not in any way be contaminated with 2ν decays. In fact, the detection of a γ ray de-excitation cascade provides an unambiguous signature for the neutrinoless decay.

5. Conclusion

The phenomenon of mixing and oscillations of atoms due to weak interaction with the violation of the total lepton number and parity was investigated. We can expect that the oscillations can be observed when the energy difference between two atomic states is small. The resonant situation can occur, if the daughter atom is in an excited atomic or/and nuclear state. The de-excitations of the final state would then proceed through the emission of X-rays (atomic structure) and/or γ -rays (nuclear structure), both of which could be used as an experimental signature for the process. The theoretical framework, which has been employed to describe these processes, is similar to that of other oscillation processes, like the oscillations of neutrinos, neutral kaons and B -mesons, or neutrons/antineutrons.

The concept was applied to the $0\nu\text{ECEC}$ process where – because of the final state excitation – mother and daughter atoms could be degenerate in mass. An experimental detection of such a process would immediately prove the Majorana nature of neutrinos. The process can, therefore, be regarded as an alternative to the $0\nu\beta^-\beta^-$ decay. A list of likely resonant transitions was provided. It was argued that accurate mass difference measurements are of paramount importance in order to

narrow down the possibilities. In fact, the precision of masses, presently at a several keV level, must be improved by at least one or two orders of magnitude. This is certainly possible given the progress made over the last years in the use of ion traps. Some examples were quoted, where mass measurements have reached accuracies ~ 10 eV.

In an ECEC process the daughter atom is left with two electron vacancies, but remains otherwise neutral. This extra atomic excitation energy was calculated using a relativistic description of the electron wave function, where the Coulomb interaction of the two holes was taken into account. In the relativistic description, parity-violating transitions from mother to daughter become possible, such as e.g., capture of an $s_{1/2}$ and a $p_{1/2}$ electron leading to the $0^+ \rightarrow 0^+$ transition. The electromagnetic and Auger decay widths of the atomic states were included in the calculations. In the case of mass degeneracy, the decay width determines the rate of transition, and the maximum rate corresponds to the unitarity limit.

The selection rules for electron capture from high orbits were obtained. We have shown that nuclear transitions with a change in the nuclear spin $\Delta J \geq 2$ are strongly suppressed. The capture of K electrons is most likely process due to the large overlap of electron wave function with the nucleus. At small distances the wave functions of $s_{1/2}$ and $p_{1/2}$ electrons have similar asymptotes, so that the capture of L_2 electrons appears to be a feasible process comparable with the K and L_1 captures. High shells are suppressed by a small value of the wave functions in the nucleus, however, these states have smaller decay widths, which compensates partly for the smallness of the unitary limit of the decay rate of the initial atoms.

Explicit formulas for the relativistic matrix elements of the 0ν ECEC were given.

We analyzed the database of the nuclei and their excited states and made a list of the most promising candidates for a resonant 0ν ECEC transition. Assuming that $|m_{\beta\beta}| = 1$ eV, we arrived at the lower bound of the normalized half-lives $\sim 10^{22}$ years, which is about a factor of 100 or 1000 below predictions for a time of $0\nu\beta^-\beta^-$ decay. Because of the uncertainty in the masses, the range of allowed half-lives is broad, and reaches several orders of magnitude. Precise measurements of the ground state masses, as well as additional spectroscopic information on the excited states (energy, spin and parity), are highly warranted to improve predictions of half-lives.

Our statistical estimates based on the data in Tables 2, 3, and 4 show that with the improvement of mass measurements and $|m_{\beta\beta}| = 1$ eV there are about 10 chances out of 100 to find transition with a normalized half-life below 10^{25} years and 50 chances out of 100 to find transition with a normalized half-life below 10^{26} years. One can expect two transitions with a normalized half-life below 10^{27} years.

Inverse transitions leading to the neutrinoless production of two bound electrons also were considered in cases of a mass degeneracy. The transitions are found to be suppressed, because the electrons would have to occupy high orbits, where the overlap with the nucleus is small.

The detection technique for identifying a 0ν ECEC-decay is rather different from the $0\nu\beta^-\beta^-$ -decay, as there is no inherent background from the 2ν -decay, which existing experiments have to cope with. Further, by exploiting the coincidence technique, in particular if the de-excitation of the nucleus proceeds through a γ -ray cascade,

a significantly improved signal to background ratio could be obtained, which would alleviate some of the demands on a low-background facility.

After submission of the manuscript, new experimental results on precision measurement of Q values and new constraints on the $0\nu\text{ECEC}$ half-lives have been reported [43, 44, 45, 46, 47].

6. Acknowledgments

This work was supported in part by the DFG projects 436 SLK 17/298, RUS 113/721/0-3, and FR601/3-1, by the Transregio Project TR27 "Neutrinos and Beyond" and the Graduiertenkolleg GRK683, by the VEGA Grant agency under the contract No. 1/0249/03, by the grant of Scientific Schools of Russian Federation No. 4568.2008.2 and the RFBR project No. 09-02-91341.

Appendix A. Electron wave function inside nucleus

The relativistic wave function of electron in the Coulomb potential has the form

$$\Psi_{\alpha m_\alpha}(\mathbf{x}) = \begin{pmatrix} f_\alpha(r)\Omega_{jlm_\alpha}(\mathbf{n}) \\ (-)^{(1+l-l')/2}g_{\alpha'}(r)\Omega_{jl'm_\alpha}(\mathbf{n}) \end{pmatrix}, \quad (\text{A.1})$$

where $\alpha = (njl)$, $\alpha' = (nj'l')$, $l' = 2j - l$, and $\Omega_{jlm}(\mathbf{n})$ are spherical spinors.

In the relativistic Coulomb problem, one can distinguish three different scales: The first scale is related to the Bohr radius $a_B = 1/(\alpha m Z)$. This scale determines the normalization of the electron wave function. The second scale $1/m$ is the Compton wavelength of an electron. Starting from these distances down to zero the upper component of Dirac wave function differs markedly from the non-relativistic Coulomb wave function. The size of the nucleus is about 500 times smaller than the Compton wavelength of an electron, so the effects associated with the finite size of the nucleus must be calculated on the basis of the relativistic Dirac equation. One may select an even smaller (third) scale. The radius of the nucleus is a few fermi, or turning to the proton, its radius is about $1 \text{ fm} \approx 1/200 \text{ MeV}^{-1}$, which is less than $\alpha/m \approx 1/70 \text{ MeV}^{-1}$. If Z increases, the radius of the nuclei $R = 1.2A^{1/3} \text{ fm}$ increases as well, but $\alpha Z/m$ is growing faster, so that $R < \alpha Z/m$ holds for all nuclei. The combination of $\alpha Z/m$ defines a third scale below which the Coulomb potential is higher than electron mass.

Asymptotics of the wave functions of electrons work for $r \lesssim 1/(2\lambda)$. Note that $\lambda \sim 1/(na_B)$ in the non-relativistic case, and $\lambda \sim m$ in the relativistic case. The nuclear radius is below $1/(2\lambda)$ and even less than $\alpha Z/(2\lambda)$. The low r approximation should therefore work very well.

In order to get the electron wave function inside the nucleus we use the asymptotic expansion of the Dirac wave function at $2\lambda r \ll 1$:

$$f_{njl}(r) \simeq \frac{\sqrt{2}\lambda^{3/2}}{\Gamma(2\gamma+1)}(\alpha Z m/\lambda - \kappa - n_r) \sqrt{\frac{(m+\varepsilon)\Gamma(2\gamma+n_r+1)\lambda}{\alpha Z m^2(\alpha Z m/\lambda - \kappa)\Gamma(n_r+1)}}(2\lambda r)^{\gamma-1},$$

$$g_{njl}(r) \simeq -\frac{\sqrt{2}\lambda^{3/2}}{\Gamma(2\gamma+1)}(\alpha Z m/\lambda - \kappa + n_r) \sqrt{\frac{(m-\varepsilon)\Gamma(2\gamma+n_r+1)\lambda}{\alpha Z m^2(\alpha Z m/\lambda - \kappa)\Gamma(n_r+1)}}(2\lambda r)^{\gamma-1}.$$

Table A.5: The upper and lower radial functions of the Dirac bi-spinors, averaged over the volume of the nucleus (in $\text{keV}^{3/2}$).

Shell	^{78}Se	^{106}Pd	^{112}Cd	^{120}Sn	^{124}Te	^{130}Xe	^{152}Sm	^{156}Gd
$1s_{1/2}$ $\langle f \rangle$	3.45×10^3	6.22×10^3	6.80×10^3	7.42×10^3	8.83×10^3	1.09×10^4	1.23×10^4	1.33×10^4
$1s_{1/2}$ $\langle g \rangle$	-4.34×10^2	-1.07×10^3	-1.23×10^3	-1.40×10^3	-1.81×10^3	-2.47×10^3	-2.94×10^3	-3.30×10^3
$2s_{1/2}$ $\langle f \rangle$	1.25×10^3	2.31×10^3	2.54×10^3	2.79×10^3	3.35×10^3	4.19×10^3	4.77×10^3	5.20×10^3
$2s_{1/2}$ $\langle g \rangle$	-1.58×10^2	-4.00×10^2	-4.59×10^2	-5.26×10^2	-6.87×10^2	-9.48×10^2	-1.14×10^3	-1.29×10^3
$3s_{1/2}$ $\langle f \rangle$	6.83×10^2	1.26×10^3	1.39×10^3	1.52×10^3	1.83×10^3	2.29×10^3	2.61×10^3	2.85×10^3
$3s_{1/2}$ $\langle g \rangle$	-8.60×10^1	-2.18×10^2	-2.51×10^2	-2.87×10^2	-3.76×10^2	-5.18×10^2	-6.23×10^2	-7.05×10^2
$4s_{1/2}$ $\langle f \rangle$	4.43×10^2	8.19×10^2	8.99×10^2	9.87×10^2	1.19×10^3	1.48×10^3	1.69×10^3	1.84×10^3
$4s_{1/2}$ $\langle g \rangle$	-5.58×10^1	-1.41×10^2	-1.63×10^2	-1.86×10^2	-2.43×10^2	-3.36×10^2	-4.04×10^2	-4.57×10^2
$2p_{1/2}$ $\langle f \rangle$	-1.72×10^1	-6.00×10^1	-7.22×10^1	-8.64×10^1	-1.23×10^2	-1.87×10^2	-2.37×10^2	-2.78×10^2
$2p_{1/2}$ $\langle g \rangle$	-1.37×10^2	-3.47×10^2	-3.99×10^2	-4.57×10^2	-5.97×10^2	-8.25×10^2	-9.92×10^2	-1.12×10^3
$2p_{3/2}$ $\langle f \rangle$	8.06×10^{-1}	2.07×10^0	2.38×10^0	2.74×10^0	3.48×10^0	4.62×10^0	5.66×10^0	6.31×10^0
$2p_{3/2}$ $\langle g \rangle$	-5.02×10^{-2}	-1.75×10^{-1}	-2.10×10^{-1}	-2.52×10^{-1}	-3.46×10^{-1}	-5.03×10^{-1}	-6.49×10^{-1}	-7.47×10^{-1}

The normalization and other conventions are those of Ref. [31]. In particular, $\gamma = \sqrt{(j + 1/2)^2 - (\alpha Z)^2}$, $\lambda = \sqrt{m^2 - \varepsilon^2}$. The radial functions are real, since $\alpha Z m - \kappa \lambda > 0$. Inside the nucleus, the screening of the charge by the electrons is weak, so Z is the charge of the unscreened nucleus.

For uniform distribution of nuclear density, the average values of the upper and lower components of the electron wave functions inside the nucleus can easily be found:

$$\begin{aligned} \langle f_{njl}(r) \rangle &= \frac{3}{\gamma + 2} f_{njl}(R), \\ \langle g_{njl}(r) \rangle &= \frac{3}{\gamma + 2} g_{njl}(R). \end{aligned}$$

At distances $r \lesssim \alpha Z/m$, the ratio (see, e.g., [31])

$$\frac{f_{njl}(R)}{g_{njl}(R)} = \frac{\alpha Z}{\gamma + \kappa} \approx \begin{cases} -\frac{2^{l+1}}{\alpha Z}, & j = l + 1/2, \\ \frac{\alpha Z}{2l}, & j = l - 1/2, \end{cases} \quad (\text{A.2})$$

is large in the $j = l + 1/2$ states and is small in the $j = l - 1/2$ states, provided $\alpha Z \ll 1$. The electron wave functions with higher values of j are suppressed inside the nucleus by additional powers of $2R\lambda \ll 1$.

In the non-relativistic theory, wave functions of particles at small distances behave like $\sim r^l$. Particles, however, become relativistic on the scale of the order of the Compton wavelength. As a result, the short distance behavior of the wave function changes. Instead of $\sim r^l$ we have $\sim r^{\gamma-1}$ ($\sim r^{j-1/2}$ for $\alpha Z \ll 1$). The suppression of the wave function at short distances is qualitatively different in non-relativistic and relativistic theories.

Table A.5 shows the upper and lower radial components of the Dirac bi-spinors, averaged over the volume of the nucleus. The values are maximum for atoms with large Z and for K electrons. One sees a significant suppression of the wave functions of $2p_{3/2}$ electrons in comparison with $1s_{1/2}$, $2p_{1/2}$, and $2s_{1/2}$ levels.

A more accurate calculation of the electron wave functions can be done on the basis of relativistic Dirac-Hartree-Fock approximation.

Appendix B. Matrix elements for capture of $s_{1/2}$ and $p_{1/2}$ bound electrons

Because of the conservation of angular momentum, transitions from the state 0^+ to the excited states of nuclei with spin J are possible only when the captured atomic electrons have total angular momentum J . The upper and lower components of Dirac bi-spinors behave at short distances as $\sim r^{\gamma-1}$, where $\gamma = \sqrt{(j+1/2)^2 - (\alpha Z)^2}$, j is the total angular momentum of electron. Wave functions of electrons with high angular momentum are strongly suppressed inside the nucleus. Increase of j by one unit leads to suppression of the electron wave function inside the nucleus by an amount $\sim R/a_B \ll 1$ where R is the size of the nucleus and a_B is the Bohr radius. Thus, we restrict ourselves to estimates of matrix elements of neutrinoless double capture of $s_{1/2}$ and $p_{1/2}$ electrons, whose wave functions are given by Eq. (A.1) with

$$\Omega_{jlm}(\mathbf{n}) = \frac{1}{\sqrt{4\pi}} \begin{cases} \chi_m, & j = 1/2, l = 0, \\ -i\boldsymbol{\sigma}\mathbf{n}\chi_m, & j = 1/2, l = 1, \end{cases} \quad (\text{B.1})$$

where χ_m are the Pauli spinors. We note that the $s_{1/2}$ wave function multiplied by γ_5 takes the form of the $p_{1/2}$ wave function if $g_{s_{1/2}}$ is replaced by $f_{p_{1/2}}$ and $f_{s_{1/2}}$ is replaced by $-g_{p_{1/2}}$.

By taking the advantage of the closure approximation the operator entering the nuclear matrix element is of the form of the product of leptonic current and two hadronic currents. We have

$$\begin{aligned} & \sum_{m_\alpha m_\beta} C_{j_\alpha m_\alpha j_\beta m_\beta}^{JM} J_\mu(\mathbf{x}_1) J_\nu(\mathbf{x}_2) (\Psi_{\alpha m_\alpha}^T(\mathbf{x}_1) C \gamma^\mu \gamma^\nu (1 - \gamma_5) \Psi_{\beta m_\beta}(\mathbf{x}_2) \\ & - \Psi_{\beta m_\beta}^T(\mathbf{x}_1) C \gamma^\mu \gamma^\nu (1 - \gamma_5) \Psi_{\alpha m_\alpha}(\mathbf{x}_2)) = (1 - (-1)^{j_\alpha + j_\beta - J}) \\ & \times \sum_{m_\alpha m_\beta} C_{j_\alpha m_\alpha j_\beta m_\beta}^{JM} \Psi_{\alpha m_\alpha}^T(\mathbf{x}_1) C \gamma^\mu \gamma^\nu (1 - \gamma_5) \Psi_{\beta m_\beta}(\mathbf{x}_2) J_\mu(\mathbf{x}_1) J_\nu(\mathbf{x}_2). \end{aligned} \quad (\text{B.2})$$

Using the non-relativistic impulse approximation and exploiting the expansion $\gamma_\mu \gamma_\nu = g_{\mu\nu} + i\sigma_{\nu\mu}$ we find

$$\begin{aligned} \gamma_\mu J^\mu(\mathbf{x}_1) \gamma_\nu J^\nu(\mathbf{x}_2) &= -g_A^2 \sum_n \sum_m \tau_n^- \tau_m^- \delta(\mathbf{x}_1 - \mathbf{x}_n) \delta(\mathbf{x}_2 - \mathbf{x}_m) \times \\ & \left[\left[-\frac{g_V^2}{g_A^2} + (\boldsymbol{\sigma}_n \cdot \boldsymbol{\sigma}_m) \right] \begin{pmatrix} 1 & 0 \\ 0 & 1 \end{pmatrix} + \frac{g_V}{g_A} \begin{pmatrix} 0 & \boldsymbol{\sigma} \\ \boldsymbol{\sigma} & 0 \end{pmatrix} \cdot (\boldsymbol{\sigma}_n - \boldsymbol{\sigma}_m) \right. \\ & \left. + \begin{pmatrix} i\boldsymbol{\sigma} & 0 \\ 0 & i\boldsymbol{\sigma} \end{pmatrix} \cdot (\boldsymbol{\sigma}_n \times \boldsymbol{\sigma}_m) \right]. \end{aligned} \quad (\text{B.3})$$

In what follows, contributions of nuclear matrix elements associated with three terms in Eq. (B.3) are supplied with subscripts S (scalar), tT (time component of the tensor), and sT (the spatial component of the tensor), respectively. The nuclear matrix elements of $0\nu\text{ECEC}$ are presented below.

Appendix B.1. $0_i^+ \rightarrow 0_f^+, 1_f^+$ nuclear transitions

The matrix element of the $0_i^+ \rightarrow 0_f^+$ nuclear transition, entering Eq. (3.20), splits into three parts

$$\mathcal{M}_{\alpha\beta}(0^+) = M_{\alpha\beta}^{(SP)}(0^+) + M_{\alpha\beta}^{(tT)}(0^+) + M_{\alpha\beta}^{(sT)}(0^+). \quad (\text{B.4})$$

where

$$\begin{aligned} M_{\alpha\beta}^{(SP)}(0^+) &= \langle 0_f^+ \parallel \sum_{n m} \tau_n^- \tau_m^- h(r_{nm}) \left[F_{\alpha\beta}^{(+)}(r_n, r_m) + G_{\alpha\beta}^{(+)}(r_n, r_m)(\hat{\mathbf{r}}_n \cdot \hat{\mathbf{r}}_m) \right] \parallel 0_i^+ \rangle, \\ &\times \left[-\frac{g_V^2}{g_A^2} + (\boldsymbol{\sigma}_n \cdot \boldsymbol{\sigma}_m) \right] \parallel 0_i^+ \rangle, \\ M_{\alpha\beta}^{(tT)}(0^+) &= i\frac{g_V}{g_A} \langle 0_f^+ \parallel \sum_{n m} \tau_n^- \tau_m^- h(r_{nm}) G_{\alpha\beta}^{(+)}(r_n, r_m) (\boldsymbol{\sigma}_n - \boldsymbol{\sigma}_m) \cdot (\hat{\mathbf{r}}_n \times \hat{\mathbf{r}}_m) \parallel 0_i^+ \rangle, \\ M_{\alpha\beta}^{(sT)}(0^+) &= \langle 0_f^+ \parallel \sum_{n m} \tau_n^- \tau_m^- h(r_{nm}) G_{\alpha\beta}^{(+)}(r_n, r_m) (\boldsymbol{\sigma}_n \times \boldsymbol{\sigma}_m) \cdot (\hat{\mathbf{r}}_n \times \hat{\mathbf{r}}_m) \parallel 0_i^+ \rangle. \end{aligned} \quad (\text{B.5})$$

The neutrino exchange potential $h(r_{nm})$ is defined in Eq. (3.24).

The transition matrix element into the 1^+ state has three components

$$\mathcal{M}_{\alpha\beta}(1^+) = M_{\alpha\beta}^{(SP)}(1^+) + M_{\alpha\beta}^{(tT)}(1^+) + M_{\alpha\beta}^{(sT)}(1^+), \quad (\text{B.6})$$

where

$$\begin{aligned} M_{\alpha\beta}^{(SP)}(1^+) &= \langle 1_f^+ \parallel \sum_{n m} \tau_n^- \tau_m^- h(r_{nm}) G_{\alpha\beta}^{(-)}(r_n, r_m) (\hat{\mathbf{r}}_n \times \hat{\mathbf{r}}_m) \parallel 0_i^+ \rangle \\ &\times \left[-\frac{g_V^2}{g_A^2} + (\boldsymbol{\sigma}_n \cdot \boldsymbol{\sigma}_m) \right] \parallel 0_i^+ \rangle \\ M_{\alpha\beta}^{(tT)}(1^+) &= i\frac{g_V}{g_A} \langle 1_f^+ \parallel \sum_{n m} \tau_n^- \tau_m^- h(r_{nm}) [F_{\alpha\beta}^{(-)}(r_n, r_m)(\boldsymbol{\sigma}_n - \boldsymbol{\sigma}_m) - G_{\alpha\beta}^{(-)}(r_n, r_m) \\ &\times [\hat{\mathbf{r}}_n \cdot \hat{\mathbf{r}}_m(\boldsymbol{\sigma}_n - \boldsymbol{\sigma}_m) + (\boldsymbol{\sigma}_n - \boldsymbol{\sigma}_m) \cdot \hat{\mathbf{r}}_m \hat{\mathbf{r}}_n - (\boldsymbol{\sigma}_n - \boldsymbol{\sigma}_m) \cdot \hat{\mathbf{r}}_n \hat{\mathbf{r}}_m] \parallel 0_i^+ \rangle \\ M_{\alpha\beta}^{(sT)}(1^+) &= \langle 1_f^+ \parallel \sum_{n m} \tau_n^- \tau_m^- h(r_{nm}) [F_{\alpha\beta}^{(-)}(r_n, r_m) \boldsymbol{\sigma}_n \times \boldsymbol{\sigma}_m - G_{\alpha\beta}^{(-)}(r_n, r_m) \\ &\times [\hat{\mathbf{r}}_n \cdot \hat{\mathbf{r}}_m \boldsymbol{\sigma}_n \times \boldsymbol{\sigma}_m - (\boldsymbol{\sigma}_n \times \boldsymbol{\sigma}_m) \cdot \hat{\mathbf{r}}_m \hat{\mathbf{r}}_n + (\boldsymbol{\sigma}_m \times \boldsymbol{\sigma}_n) \cdot \hat{\mathbf{r}}_n \hat{\mathbf{r}}_m] \parallel 0_i^+ \rangle. \end{aligned} \quad (\text{B.7})$$

The functions $F_{\alpha\beta}^{(\pm)}(r_n, r_m)$ and $G_{\alpha\beta}^{(\pm)}(r_n, r_m)$ depend on the quantum numbers of the captured electrons

$$\begin{aligned} \frac{8\pi F_{\alpha\beta}^{(\pm)}(r_n, r_m)}{\sqrt{2}} &= \begin{cases} f_\alpha(r_n)f_\beta(r_m) \pm f_\beta(r_n)f_\alpha(r_m), & (n_\alpha s_{1/2}, n_\beta s_{1/2}), \\ (f_\alpha(r_n)g_\beta(r_m) \pm g_\beta(r_n)f_\alpha(r_m))/2 \\ \pm (f_\beta(r_n)g_\alpha(r_m) \pm g_\alpha(r_n)f_\beta(r_m))/2, & (n_\alpha s_{1/2}, n_\beta p_{1/2}), \\ g_\alpha(r_n)g_\beta(r_m) \pm g_\beta(r_n)g_\alpha(r_m), & (n_\alpha p_{1/2}, n_\beta p_{1/2}), \end{cases} \\ \frac{8\pi G_{\alpha\beta}^{(\pm)}(r_n, r_m)}{\sqrt{2}} &= \begin{cases} g_\alpha(r_n)g_\beta(r_m) \pm g_\beta(r_n)g_\alpha(r_m), & (n_\alpha s_{1/2}, n_\beta s_{1/2}), \\ (-g_\alpha(r_n)f_\beta(r_m) \mp f_\beta(r_n)g_\alpha(r_m))/2 \\ \pm (-g_\beta(r_n)f_\alpha(r_m) \mp f_\alpha(r_n)g_\beta(r_m))/2, & (n_\alpha s_{1/2}, n_\beta p_{1/2}), \\ f_\alpha(r_n)f_\beta(r_m) \pm f_\beta(r_n)f_\alpha(r_m), & (n_\alpha p_{1/2}, n_\beta p_{1/2}). \end{cases} \end{aligned}$$

If the electrons have the same quantum numbers $\alpha = \beta$, these functions should be divided further by $\sqrt{2}$.

It is worthwhile to note that for $\alpha = \beta$ (e.g., capture of two K electrons) $F_{\alpha\beta}^{(-)}(r_n, r_m)$ and $G_{\alpha\beta}^{(-)}(r_n, r_m)$ vanish.

Averaging of these functions over the nucleus with the unit weight also gives a zero result. However, these functions are multiplied by the nuclear matrix elements that are antisymmetric under permutation of the arguments. The outcome, therefore, is different from zero, although the naive factorization produces a vanishing result.

A reasonable estimate can be obtained on the basis of Cauchy's inequality. Let a_{ij} and b_{ij} be antisymmetric tensors. The upper limit of the sum $\sum_{ij} a_{ij}b_{ij}$ can be evaluated from

$$\sum_{ij} a_{ij}b_{ij} \leq \left(\sum_{ij} a_{ij}^2 \right)^{1/2} \times \left(\sum_{ij} b_{ij}^2 \right)^{1/2}.$$

As an estimate of the matrix element we take the upper limit that splits into a product of the lepton and nuclear parts. Combinations of the electron wave functions entering the matrix elements of $0_i^+ \rightarrow 0_f^\pm$ and 1_f^\pm transitions are given in Table 1.

Appendix B.2. $0_i^+ \rightarrow 0_f^-, 1_f^-$ nuclear transitions

The matrix element decomposes into a sum of two parts that have different tensor structure:

$$\mathcal{M}_{\alpha\beta}(0^-) = M_{\alpha\beta}^{(tT)}(0^-) + M_{\alpha\beta}^{(sT)}(0^-), \quad (\text{B.8})$$

where

$$\begin{aligned} M_{\alpha\beta}^{(tT)}(0^-) &= i \frac{g_V}{g_A} \langle 0_f^- \parallel \sum_{n m} \tau_n^- \tau_m^- h(r_{nm}) \\ &\times \left[\left(H_{\alpha\beta}^{(+)}(r_n, r_m) \hat{\mathbf{r}}_n - H_{\alpha\beta}^{(+)}(r_m, r_n) \hat{\mathbf{r}}_m \right) \cdot (\boldsymbol{\sigma}_n - \boldsymbol{\sigma}_m) \right] \parallel 0_i^+ \rangle, \\ M_{\alpha\beta}^{(sT)}(0^-) &= \langle 0_f^- \parallel \sum_{n m} \tau_n^- \tau_m^- h(r_{nm}) \\ &\times \left[\left(H_{\alpha\beta}^{(+)}(r_n, r_m) \hat{\mathbf{r}}_n - H_{\alpha\beta}^{(+)}(r_m, r_n) \hat{\mathbf{r}}_m \right) \cdot (\boldsymbol{\sigma}_n \times \boldsymbol{\sigma}_m) \right] \parallel 0_i^+ \rangle. \end{aligned} \quad (\text{B.9})$$

The transition matrix element of the vector type splits into a sum of three parts:

$$\mathcal{M}_{\alpha\beta}(1^-) = M_{\alpha\beta}^{(SP)}(1^-) + M_{\alpha\beta}^{(tT)}(1^-) + M_{\alpha\beta}^{(sT)}(1^-), \quad (\text{B.10})$$

where

$$\begin{aligned} M_{\alpha\beta}^{(SP)}(1^-) &= - \langle 1_f^- \parallel \sum_{n m} \tau_n^- \tau_m^- h(r_{nm}) \\ &\times \left[H_{\alpha\beta}^{(-)}(r_n, r_m) \hat{\mathbf{r}}_n - H_{\alpha\beta}^{(-)}(r_m, r_n) \hat{\mathbf{r}}_m \right] \left[-\frac{g_V^2}{g_A^2} + (\boldsymbol{\sigma}_n \cdot \boldsymbol{\sigma}_m) \right] \parallel 0_i^+ \rangle, \\ M_{\alpha\beta}^{(tT)}(1^-) &= i \frac{g_V}{g_A} \langle 1_f^- \parallel \sum_{n m} \tau_n^- \tau_m^- h(r_{nm}) \\ &\times \left[H_{\alpha\beta}^{(-)}(r_n, r_m) \hat{\mathbf{r}}_n \times (\boldsymbol{\sigma}_n - \boldsymbol{\sigma}_m) - H_{\alpha\beta}^{(-)}(r_m, r_n) \hat{\mathbf{r}}_m \times (\boldsymbol{\sigma}_m - \boldsymbol{\sigma}_n) \right] \parallel 0_i^+ \rangle, \end{aligned} \quad (\text{B.11})$$

$$M_{\alpha\beta}^{(sT)}(1^-) = \langle 1_f^- \parallel \sum_{n m} \tau_n^- \tau_m^- h(r_{nm}) \times \left[H_{\alpha\beta}^{(-)}(r_n, r_m) \hat{\mathbf{r}}_n \times (\boldsymbol{\sigma}_n \times \boldsymbol{\sigma}_m) - H_{\alpha\beta}^{(-)}(r_m, r_n) \hat{\mathbf{r}}_m \times (\boldsymbol{\sigma}_m \times \boldsymbol{\sigma}_n) \right] \parallel 0_i^+ \rangle.$$

The functions $H_{\alpha\beta}^{(\pm)}(r_n, r_m)$ have the form

$$\frac{8\pi H_{\alpha\beta}^{(\pm)}(r_n, r_m)}{\sqrt{2}} = \begin{cases} g_\alpha(r_n) f_\beta(r_m) \pm g_\beta(r_n) f_\alpha(r_m), & (n_\alpha s_{1/2}, n_\beta s_{1/2}), \\ (g_\alpha(r_n) g_\beta(r_m) \mp f_\beta(r_n) f_\alpha(r_m))/2 & \\ \pm (g_\beta(r_n) g_\alpha(r_m) \mp f_\alpha(r_n) f_\beta(r_m))/2, & (n_\alpha s_{1/2}, n_\beta p_{1/2}), \\ f_\alpha(r_n) g_\beta(r_m) \pm f_\beta(r_n) g_\alpha(r_m), & (n_\alpha p_{1/2}, n_\beta p_{1/2}). \end{cases}$$

If $\alpha = \beta$, then the functions should be divided by $\sqrt{2}$. For $\alpha = \beta$ (e.g., capture of two electrons from the K-shell), the averaged matrix element of $H_{\alpha\beta}^{(-)}(r_n, r_m)$ vanishes.

It is important to note that due to parity violation, the transitions into the 0_f^- states with the capture of two $s_{1/2}$ electrons are allowed, as well as the transitions into the 0_f^+ states with the capture of one $s_{1/2}$ and one $p_{1/2}$ electrons.

The functions $H_{\alpha\beta}^{(+)}(r_n, r_m)$ and $H_{\alpha\beta}^{(-)}(r_n, r_m)$ are explicitly symmetric and anti-symmetric with respect to the indices n and m . They are multiplied by the nuclear part of the operator, which has the same symmetry properties. Factorization of the transition amplitude $0_i^+ \rightarrow 0_i^-$ is possible, since the combination of electron wave functions is averaged over the nuclear volume with a unit weight. The nuclear matrix element equals (3.23).

In the transition $0_i^+ \rightarrow 1_f^-$ we encounter the same problem as in the transition $0_i^+ \rightarrow 1_f^+$. The nuclear part of the operator is antisymmetric, so the straightforward factorization is impossible. We again restrict ourselves to estimate the upper limit on the matrix element squared. Before the estimate we must, however, take into account that only the antisymmetric part of $H_{\alpha\beta}^{(-)}(r_n, r_m)$ contributes to the amplitude, therefore, the value of

$$(H_{\alpha\beta}^{(-)}(r_n, r_m) - H_{\alpha\beta}^{(-)}(r_m, r_n))^2/4$$

must be averaged.

The leptonic parts of the matrix elements discussed above are shown in Table 1.

References

- [1] W.H. Furry, Phys. Rev, **56** (1939) 1184.
- [2] J. Schechter and J.W.F. Valle, Phys. Rev. D **25** (1982) 2951; M. Hirsch, H.V. Klapdor-Kleingrothaus, and S. Kovalenko, Phys. Lett. B **372** (1996) 8.
- [3] W.C. Haxton and G.S. Stephenson, Prog. Part. Nucl. Phys. **12** (1984) 409; M. Doi, T. Kotani and E. Takasugi, Prog. Theor. Phys. (Supp.) **83** (1985) 1; A. Faessler and F. Šimkovic, J. Phys. G **24** (1998) 2139; J. Suhonen and O. Civitarese, Phys. Rept. **300** (1998) 123; S.R. Elliott and P. Vogel, Annu. Rev.

- Nucl. Part. Sci. **52** (2002) 115; J.D. Vergados, Phys. Rep. **361** (2002) 1; V.I. Tretyak and Yu.G. Zdesenko, At. Dat. Nucl. Dat. Tabl. **80** (2002) 83; S.R. Elliott, J. Engel, J. Phys. G **30** (2004) R183; A.S. Barabash, Phys. Atom. Nucl. **70** (2007) 1191.
- [4] H.V. Klapdor-Kleingrothaus, I.V. Krivosheina, Mod. Phys. Lett. A **21** (2006) 1547; H.V. Klapdor-Kleingrothaus, A. Dietz, H.L. Harney, I.V. Krivosheina, Mod. Phys. Lett. A **16** (2001) 2409.
- [5] F. Šimkovic, A. Faessler, H. Mütter, V. Rodin, and M. Stauf, Phys. Rev. C **79** (2009) 055501.
- [6] I. Abt et al. (GERDA Collaboration), arXiv:hep-ex/0404039; J. Jochum, Prog. Part. Nucl. Phys. **64** (2010) 261.
- [7] F.T. Avignone, S.R. Elliott, and J. Engel, Rev. Mod. Phys. **80** (2008) 481.
- [8] S.M. Bilenky, A. Faessler, and F. Šimkovic, Phys. Rev. D **70** (2004) 033003; S.M. Bilenky, A. Faessler, T. Gutsche, and F. Šimkovic, Phys. Rev. D **72** (2005) 053015.
- [9] S. Pascoli and S.T. Petcov, Phys. Rev. D **77** (2008) 113003.
- [10] Z. Sujkowski and S. Wycech, Phys. Rev. C **70** (2004) 052501; L. Lukaszuk, Z. Sujkowski and S. Wycech, Eur. Phys. J A **27** (2006) 63.
- [11] D. Frekers, *Preprint* hep-ex/0506002.
- [12] A.S. Barabash, Ph. Hubert, A. Nachab, and V. Umatov, Nucl. Phys. A **785** (2007) 371.
- [13] A.S. Barabash, Ph. Hubert, A. Nachab, S.I. Konovalov, I.A. Vanyushin, and V.I. Umatov, Nucl. Phys. A **807** (2008) 269.
- [14] R.G. Winter, Phys. Rev. **1000** (1955) 142.
- [15] J. Bernabéu, A. De Rujula, and C. Jarlskog, Nucl. Phys. B **223** (1983) 15.
- [16] S. Rahaman et al., Phys. Rev. Lett. **103** (2009) 042501.
- [17] V.S. Kolhinen et al., Phys. Lett B **684** (2010) 17.
- [18] K. Blaum, Phys. Rep. **425** (2006) 1.
- [19] M. Redshaw et al., Phys. Rev. Lett. **102** (2009) 212502; Phys. Rev. Lett. **98** (2007) 053003.
- [20] G. Douysset et al., Phys. Rev. Lett. **86** (2001) 4259.
- [21] N.D. Scielzo et al., Phys. Rev. C **80** (2009) 0225501.

- [22] F. Šimkovic, M.I. Krivoruchenko, Phys. Part. Nucl. Lett. **6** (2009) 298.
- [23] L.B. Okun, *Leptons and Quarks*, (North-Holland, Amsterdam, 1984).
- [24] C.B. Dover, A. Gal, J.M. Richard, Phys. Rev. D **27** (1983) 1090; Phys. Rev. C **31** (1985) 1423.
- [25] M.I. Krivoruchenko, Yad. Fiz. **59** (1996) 2046 [Phys. Atom. Nucl. **59** (1996) 1972].
- [26] M.C. Gonzalez-Garcia, M. Maltoni, Phys. Lett. B **663** (2008) 405.
- [27] L.D. Landau and E.M. Lifschitz, *Quantum Mechanics. Non-relativistic Theory*, 3-rd ed. (Nauka, Moscow, 1974).
- [28] F.B. Larkins, At. Data and Nucl. Data Tables **20** (1977) 313.
- [29] J.L. Campbell and T. Papp, At. Data and Nuclear Data Tables **77** (2001) 1.
- [30] F. Šimkovic, M.I. Krivoruchenko, A. Faessler, Prog. Part. Nucl. Phys. **66** (2011) 446.
- [31] V.B. Berestetsky, E.M. Lifshitz, L.P. Pitaevsky, *Quantum Electrodynamics*, 2-nd ed. (Nauka, Moscow, 1986).
- [32] Hans A. Bethe und Edwin E. Salpeter, *Quantum Mechanics of One- And Two-Electron Atoms* , (Springer-Verlag, Berlin 1957).
- [33] Center for Nuclear Studies, Department of Physics, The George Washington University. Data Analysis Center: <http://www.nndc.bnl.gov/>
- [34] J. Suhonen, Phys. Rev. C **62** (2000) 042501.
- [35] V. Kolhinen et al., Phys. Lett. B **697** (2011) 116.
- [36] C. Arnaboldi et al. (CUORE Collaboration), Phys. Rev. C **78** (2008) 035502. A. Giuliani, Acta Phys. Polon. B **41** (2010) 1447.
- [37] J.V. Dawson et al. (COBRA collaboration), Phys. Rev. C **80** (2009) 025502; K. Zuber, Prog. Part. Nucl. Phys. **64** (2010) 267.
- [38] Ch. Briancon et al. (TGV Collaboration), AIP Conf. Proc. **1180** (2009) 107. N.I. Rukhadze et al., J. Phys. Conf. Ser. **203** (2010) 012072.
- [39] I.I. Sobelman, *Introduction to the Theory of Atomic Spectra*, (Pergamon Press, Oxford, 1972).
- [40] D.M. Riffe, G.K. Wertheim, D.N. Buchanan, and P.H. Citrin, Phys. Rev. B **45** (1992) 6216.
- [41] D.A. Shirley, R.L. Martin, S.P. Kowalczyk, F.R. McFeely, and L. Ley, Phys. Rev. B **15** (1977) 544.

- [42] P. Domin, S.G. Kovalenko, F. Šimkovic, S.V. Semenov, Nucl. Phys. A **753** (2005) 337.
- [43] S. Eliseev *et al.*, Phys. Rev. Lett. **106** (2011) 052504.
- [44] N.I. Rukhadze *et al.*, Nucl. Phys. A **852** (2011) 197.
- [45] S. Eliseev *et al.*, Phys. Rev. C **83** (2011) 038501.
- [46] V.S. Kolhinen *et al.*, Phys. Lett. B **697** (2011) 116.
- [47] P. Belli *et al.*, Nucl. Phys. A **859** (2011) 126.